RESEARCH ARTICLE

Organismal responses to deteriorating water quality during the historic 2020 red tide off Southern California

Zachary R. Skelton[1,2,*], Lillian R. McCormick[1,†], Garfield T. Kwan[1,3,†], Joshua Lonthair[3,4], Carlos Neira[1], Samantha M. Clements[1], Todd R. Martz[1], Philip J. Bresnahan[5], Uwe Send[1], Sarah N. Giddings[1], Jeffrey C. Sevadjian[1], Stephanie Jaeger[6], Adriano Feit[6], Benjamin W. Frable[1], Phillip J. Zerofski[1], Melissa Torres[1], Jeffrey A. Crooks[1,7], Justin McCullough[7], Melissa L. Carter[1], Eva Ternon[1,8], Luke P. Miller[9], Gabriella M. Kalbach[9], Duncan C. Wheeler[1], P. Ed Parnell[1], Katherine M. Swiney[3], Garrett Seibert[2], Jeremiah J. Minich[1], John R. Hyde[3], Philip A. Hastings[1], Jennifer E. Smith[1], Lisa M. Komoroske[4], Martin Tresguerres[1], Lisa A. Levin[1], and Nicholas C. Wegner[3]

In April and May of 2020, a large phytoplankton bloom composed primarily of the dinoflagellate *Lingulodinium polyedra* reached historic levels in geographic expanse, duration, and density along the coast of southern California, United States, and Baja California Norte, Mexico. Here, we report the water quality parameters of dissolved oxygen and pH over the course of the red tide, as measured by multiple sensors deployed in various locations along San Diego County, and document the extent of mass organism mortality using field surveys and community science observations. We found that dissolved oxygen and pH corresponded with bloom dynamics, with extreme hypoxic and hyperoxic conditions occurring at multiple locations along the coast, most notably within select estuaries where dissolved oxygen reached 0 mg L^{-1} and hypoxia occurred for up to 254 consecutive hours, as well as along the inner shelf of the open coast where dissolved oxygen dropped as low as 0.05 mg L^{-1}. Similarly, pH ranged widely (6.90–8.79) across the bloom over both space and time, largely corresponding with dissolved oxygen level. Extreme changes in dissolved oxygen and pH, in addition to changes to other water parameters that affect organismal health, ultimately led to documented mortalities of thousands of demersal and benthic fishes and invertebrates (primarily within estuarine and inner-shelf environments), and long-term surveys within one lagoon showed protracted changes to benthic infaunal density and species composition. In addition to field observations, we also quantified water quality parameters and organism mortalities from four local aquarium facilities, with varying levels of filtration and artificial oxygenation, and documented the morphological changes in the gills of captive-held Pacific sardine in response to the red tide. We show that multiple factors contributed to organismal stress, with hypoxia likely being the most widespread, but not the only, cause of mortality.

Keywords: Estuary, Fish gill, Fish kill, Harmful algal bloom, Hypoxia, Ionocyte, Mass mortality

[1] Scripps Institution of Oceanography, University of California San Diego, La Jolla, CA, USA

[2] Ocean Associates Inc. under contract to Fisheries Resources Division, Southwest Fisheries Science Center, National Marine Fisheries Service, National Oceanic and Atmospheric Administration, La Jolla, CA, USA

[3] Fisheries Resources Division, Southwest Fisheries Science Center, National Marine Fisheries Service, National Oceanic and Atmospheric Administration, La Jolla, CA, USA

[4] Department of Environmental Conservation, University of Massachusetts Amherst, Amherst, MA, USA

[5] Department of Earth and Ocean Sciences, University of North Carolina Wilmington, Wilmington, NC, USA

[6] Environmental Monitoring and Technical Services Division, Public Utilities Department, City of San Diego, San Diego, CA, USA

[7] Tijuana River National Estuarine Research Reserve, Imperial Beach, CA, USA

[8] Laboratoire d'Océanographie de Villefranche sur mer (UMR 7093), Sorbonne Université, CNRS, Villefranche-sur-mer, France

[9] Coastal and Marine Institute Laboratory, San Diego State University, San Diego, CA, USA

[†] These two authors contributed equally to this work.

[*] Corresponding author:
Emails: zskelton@ucsd.edu; zachary.skelton@noaa.gov

Introduction

Coastal phytoplankton blooms, including those known as "red tides," often lead to abrupt changes in the physical marine environment that impact local ecology (Glibert et al., 2001; Landsberg et al., 2005; Hallett et al., 2016) and can have negative economic and public health effects (Anderson, 1994; Hoagland and Scatasta, 2006; Jin et al., 2008; Lewitus et al., 2012; Zohdi and Abbaspour, 2019). For example, low oxygen conditions (Dupont et al., 2010; Gravinese et al., 2020), low pH (Leivestad and Muniz, 1976; Ochumba, 1990), algal toxins (Scholin et al., 2000; Fire and Van Dolah, 2012), altered geochemical cycles of contaminants (Pickhardt et al., 2002; Achá et al., 2018), and combinations of these factors during red tide events can adversely affect organismal health and lead to mortality. For this reason, red tides are often called harmful algal blooms, and although they occur naturally, anthropogenic activities have exacerbated their frequency and intensity through increases in ocean temperature, storm events, and nutrient inputs (Anderson et al., 2002; Hallegraeff, 2010; Wells et al., 2015; Grattan et al., 2016; Baohong et al., 2021).

In southern California, red tides that span days to months have been observed since long-term monitoring began at Scripps Institution of Oceanography (SIO) in the early 1900s (e.g., Torrey, 1902; Allen, 1946; Holmes et al., 1967; Kahru and Mitchell, 1998; Omand et al., 2011). In April and May 2020, an unusual red tide dominated by the mixotrophic dinoflagellate *Lingulodinium polyedra* (previously *Gonyaulax polyedra*) spanned over 400 km from approximately Bahía de Todos Santos, Ensenada, Baja California Norte, Mexico, to Goleta, California, USA (**Figure 1**) and resulted in one of the most prolonged and widespread red tide events in recorded history off the coast of southern California (Anderson and Hepner-Medina, 2020; Kahru et al., 2021). In addition, the observed density of *L. polyedra* was unprecedented. Since approximately 1900, the maximum density of *L. polyedra* recorded at SIO was 1 million cells L^{-1}; whereas on April 30, 2020, the maximum density reached over 29 million cells L^{-1} (Ternon et al., 2023). This high density led to extreme red-brown coloration of seawater during the day (**Figure 2A**) and intense bioluminescence at night (**Figure 2B**).

The phytoplankton bloom was first recorded by a surface water Imaging FlowCytobot (IFCB115) at the Del Mar Mooring (32.9294°, −117.3172°), approximately 5 km offshore on March 31, 2020, and consisted primarily of chain-forming diatoms such as *Chaetoceros* spp. and *Pseudo-nitzschia* spp. at its conception. These chain-forming diatoms were quickly replaced by *Lingulodinium polyedra*, and to a lesser extent by other dinoflagellates such as *Gonyaulax* spp., *Ceratium* spp., and *Protoperidinium* spp. Abnormally high precipitation (reaching 400% above typical rainfall levels) in late March and early April (see figure 3G from Shipley et al., 2022, and National Oceanic and Atmospheric Administration [NOAA] National Weather Service database for more details), coupled with warm water conditions during this same time period, likely led to stratification of surface
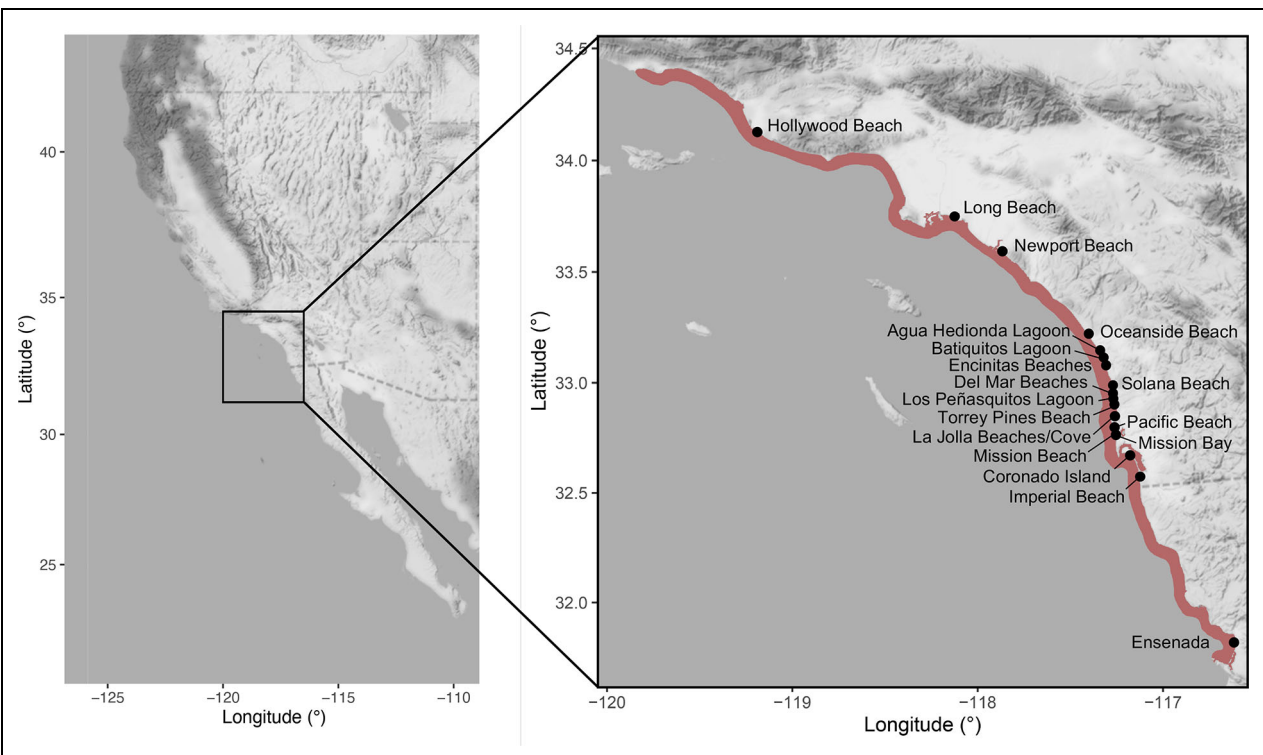
Figure 1. Range of the 2020 red tide and mass mortality sites. Maximum extent of the 2020 red tide (red shading) along the coast of southern California, USA, and northern Baja California, Mexico, and localities of reported fish and invertebrate mortality (black circles). Figure created using *ggmap* package (Kahle and Wickham, 2013) in R and Adobe Photoshop version 24.1.1.

Figure 2. Digital images showing aspects of the historic 2020 red tide. (A) Surfer in the thick red-brown water caused by a high density of *Lingulodinium polyedra* off the Scripps Institution of Oceanography (SIO) pier (Dr. Michael Latz, SIO, April 24, 2020). (B) Bioluminescence of *L. polyedra* caused by wave disturbance off the SIO pier (Kevin Key Photography, San Diego, May 14, 2020). Bacterial mats formed on (C) the shore of Agua Hedionda Lagoon after a mass mortality event (S Anthony, May 10, 2020), and (D) the subtidal sediments of La Jolla Canyon (Raph Beresh, May 9, 2020). (E) A close up of a decaying Pacific oyster (*Magallana gigas*) and surrounding bacterial mat in Los Peñasquitos Lagoon (Carlos Neira, May 20, 2020). (F) Organic-rich sea foam at Scripps beach caused by decay of bloom (Zach Skelton, May 19, 2020).

waters that allowed *L. polyedra* to thrive and persist (Zheng et al., 2023). While offshore bloom formation indicates that terrestrial runoff of nutrients was not the primary cause initiating the bloom, nutrient runoff likely helped to sustain and intensify phytoplankton growth in the following weeks (Anderson and Hepner-Medina, 2020). As the bloom began decaying from early to mid-May, microbial mats were observed along the shoreline and subtidal sediments at depths down to 40 m (**Figure 2C–E**). In addition, large amounts of seafoam formed due to the high amounts of suspended organic material (**Figure 2F**). Simultaneously, the release of sulfuric compounds as a byproduct of decay was evident by smell for several weeks. The red tide led to extreme changes in environmental water parameters and culminated in large-scale mass mortalities of marine organisms that spanned across the geographic range of the bloom.

In this study, we correlated physical oceanographic data for oxygen and pH from various near-shore monitoring stations with spatiotemporal mortality data for wild marine organisms in an effort to quantify the biological impacts of this historic red tide. We also examined the impacts of the red tide on organisms housed within several local aquarium facilities utilizing various levels of filtration and artificial oxygenation of flow-through seawater in an attempt to understand the potential factors leading to organismal stress and mortality. We further assessed the responses of Pacific sardine (*Sardinops sagax*) that were reared in one facility and sampled before and during red tide exposure. We were particularly interested in gill responses as (1) the gill comprises a substantial proportion of surface area exposed to the environment, and (2) the gill serves as the primary site of gas exchange and ion-transport to maintain homeostasis via specialized ion-transporting cells called ionocytes. Thus, we searched for physical damage to the gill ultrastructure and for indicators of change in ion-transport capacity in gill ionocytes. This compilation of field observations, aquarium case studies, and laboratory analyses provides a snapshot of the multitude of stressors present during this unusual red tide event and their implications for organisms, ecosystems, and facilities with flow-through seawater systems.

Methods

Environmental dynamics

We collated dissolved oxygen, pH, and temperature data from 11 subsurface sensor packages that were collecting long-term oceanographic data at seven different locations along the coast of San Diego County from March 1 to June 30, 2020 (**Figure 3A**) to provide a spatial and temporal summary of the oceanographic conditions throughout the red tide (see Table S1 for additional sensor information). For descriptive comparison, we organized these sensor data by location and depth into the following categories:
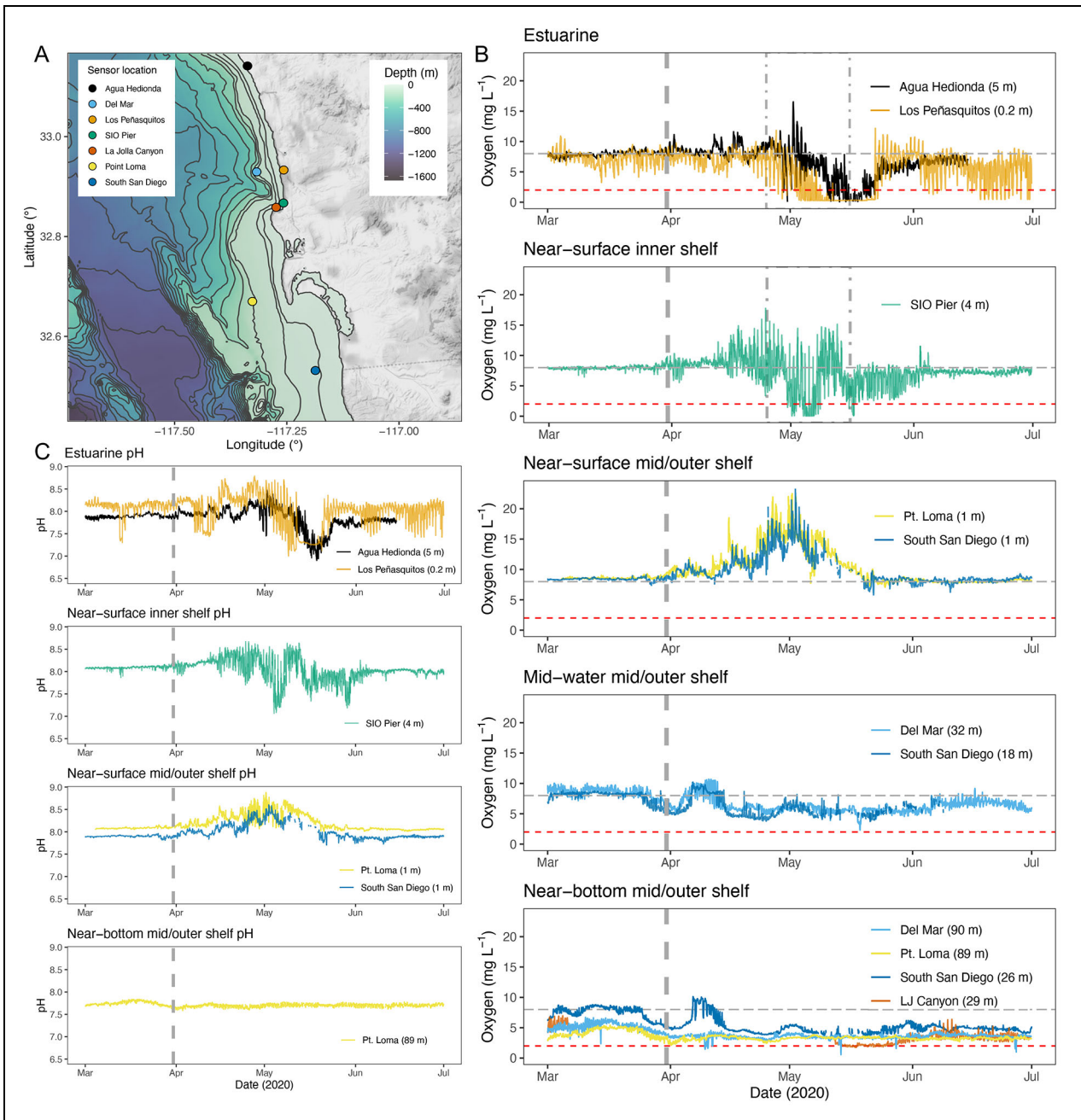
Figure 3. Changes in dissolved oxygen and pH at various sites across the 2020 red tide. (A) Site map showing sensor locations along the coast of San Diego County, California, USA. Water depth contour lines (black lines and color scale) show 0 m, 25 m, 50 m, 100 m, and then at each 100-m interval. (B) Dissolved oxygen concentrations (mg L^{-1}) at all sites separated into categories by location and depth: estuarine, near-surface inner shelf, near-surface mid/outer shelf, mid-water mid/outer shelf, and near-bottom mid/outer shelf. Hypoxia was defined as oxygen <2 mg L^{-1} (approximately 25% air saturation depending on temperature and salinity; horizontal dashed red line). A reference for 100% oxygen saturation is placed at 8 mg L^{-1} (horizontal dashed gray line); the exact value may vary by ± 2 mg L^{-1} depending on the temperature and salinity at each sensor location. Dash-dot gray box represents the date range used for a more detailed view of the dissolved oxygen concentrations during the height of red tide-induced mortalities shown in **Figure 4**. (C) Subsurface pH profiles during the red tide from estuarine, near-surface inner shelf, near-surface mid/outer shelf, and near-bottom mid/outer shelf sites. For (B) and (C), bloom initiation (vertical dashed gray line) was defined by a rise in *Lingulodinium* polyedra concentration captured by the Imaging FlowCytobot attached to the Del Mar mooring. Figures created using the *ggmap* (Kahle and Wickham, 2013) and *ggplot2* (Wickham, 2016) packages in R.

estuarine (partially enclosed bodies of water), with sensor depths of 0.2–5 m and water column depths of 1.5–6 m; near-surface inner shelf, with 4 m sensor depth and 6 m

water column depth; near-surface mid/outer shelf, with 1 m sensor depth and 30–95 m bottom depth; mid-water mid/outer shelf, with 18–32 m sensor depth and 30–100 m
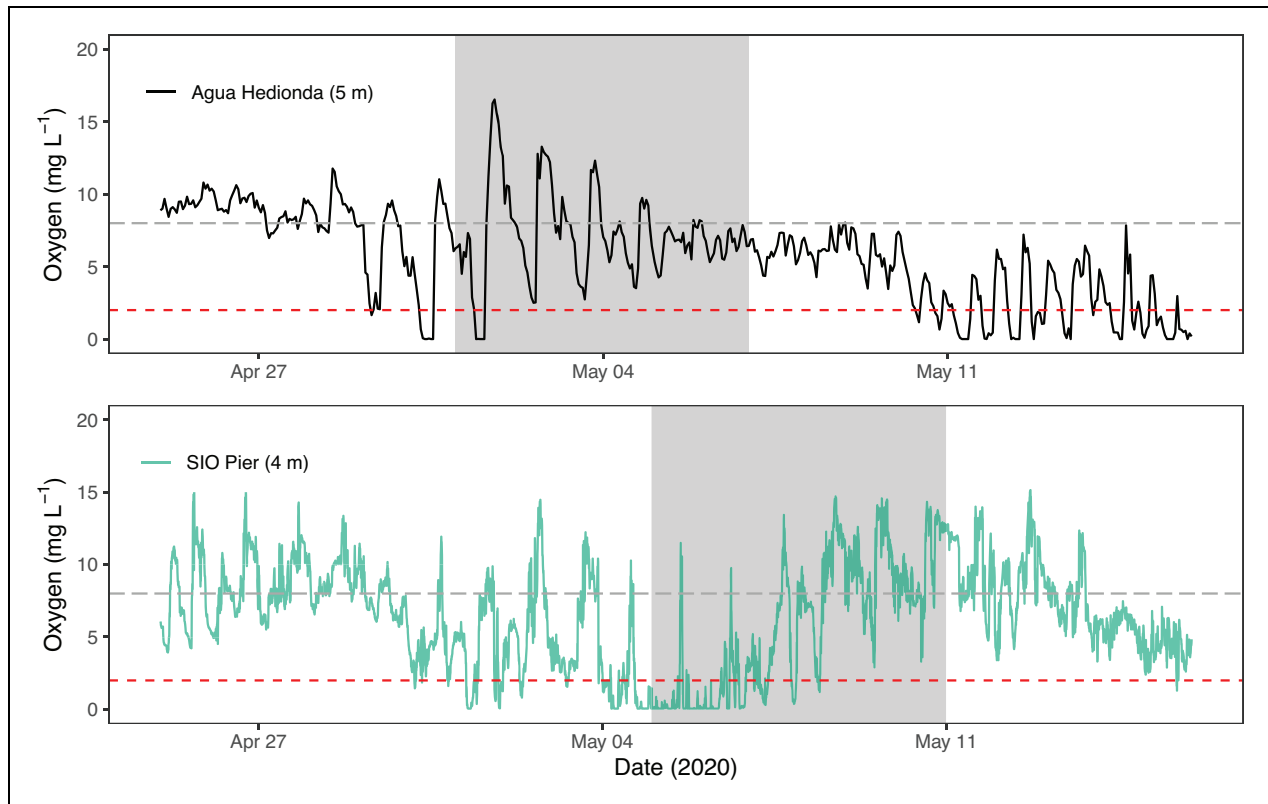
Figure 4. Diurnal oxygen variability (mg L^{-1}) between April 25 and May 15, 2020, showing the period of high red-tide mortality at an estuarine and inner shelf site. Hypoxia was defined as oxygen <2 mg L^{-1} (approximately 25% air saturation; horizontal dashed red line). A reference for 100% air saturation was placed at 8 mg L^{-1} (horizontal dashed gray line); the exact value may vary by $\pm$ 2 mg L^{-1} depending on the temperature and salinity at each sensor location. Gray shaded boxes indicate the period of reported mortalities at each location.

bottom depth; and near-bottom mid/outer shelf, with 29–90 m sensor depth and 30–100 m bottom depth. Specifically, sensor locations and approximate depths, which can vary slightly with tide, especially within the estuarine and inner shelf environments, included Agua Hedionda Lagoon (33.1415°, −117.3377°), with 5 m sensor depth and 6 m bottom depth; Del Mar (32.9294°, −117.3172°), with 32 m and 90 m sensor depths and 100 m bottom depth; Los Peñasquitos Lagoon (32.9335°, −117.2570°), with 0.2 m sensor depth and 1.5 m bottom depth; SIO Pier (32.8671°, −117.2575°), with 4 m sensor depth and 6 m bottom depth; La Jolla Canyon (32.8584°, −117.2739°), with 29 m sensor depth and 30 m bottom depth; Point Loma (32.6696°, −117.3230°), with 1 m and 89 m sensor depths and 95 m bottom depth; and South San Diego (32.5319°, −117.1864°), with 1 m, 18 m, and 26 m sensor depths and 30 m bottom depth.

We report dissolved oxygen measurements throughout the manuscript in mg L^{-1} as well as percent saturation (% sat), which allows for comparison of the relative amount (percentage) of expected oxygen across sites when considering differences in temperature and salinity. We define "hypoxia" as a dissolved oxygen concentration <2 mg L^{-1} (approximately 25% sat depending on the corresponding temperature and salinity), while acknowledging that many marine species experience adverse effects of low oxygen at

values above 2 mg L^{-1} (Vaquer-Sunyer and Duarte, 2008). We report the maximum measured values of oxygen saturation levels from all sensors, which in some cases extend far past the factory measurement upper range (120%– 150% sat). Oxygen levels that exceeded these upper range values may therefore be less accurate but are included to show approximate oxygen levels.

Biological impacts
Field observations
Marine fish and invertebrate strandings and mortalities were reported along the coastline over almost the entire geographic extent of the red tide, with large die-offs starting on May 2, 2020. Due to COVID-19 restrictions and both California state and institutional stay-at-home mandates, we collected many of our first mass-mortality observations through community science. Specifically, we obtained photographic observations and videos from the community via email, social media (*Instagram* and *Facebook*), and through the website *iNaturalist* (www.inaturalist.org). When we received clearance to conduct field work (shortly after the height of observed mass mortality events), we observed and photographed beached organisms at various locations along the coast on May 5 (La Jolla Beaches/Cove, Pacific Beach, Mission Bay, Mission Beach), and May 6 (Agua Hedionda Lagoon, Solana Beach, Encinitas Beaches, Del

Mar Beach and the San Dieguito River mouth). For both community science data and our direct observations, we identified organisms to the lowest taxonomic rank (species, where possible) and grouped them into abundance bins of <10 (1s), 10–99 (10s), 100–999 (100s), and 1000+ (1000s). We also categorized identified species by observation location (open coast versus estuarine) and ecotype: benthic, demersal, pelagic for fishes (informed by *FishBase* at www.fishbase.org; Froese and Pauly, 2023), in-substrate, sessile, benthic, pelagic for invertebrates (*SeaLifeBase* at www.sealifebase.org; Palomares and Pauly, 2023), and semi-aquatic and terrestrial for birds (*AviBase* at https://avibase.bsc-eoc.org/; Lepage et al., 2014).

In addition to reports of organismal mortality, we analyzed data from an ongoing assessment of soft-sediment benthic invertebrate density within Los Peñasquitos Lagoon pre-red tide (March 3, 2020), during the red tide (May 5 and May 28, 2020) and post-red tide (July 1 and August 17, 2020). We sampled macrobenthic organisms (>300 μm) using 5 cm deep benthic cores (area of 18.1 cm^2) collected in triplicate from each of three established stations within the lagoon: (1) Northwest (NW) near-ocean station (32.9333°; 117.2572°), which is closest to the lagoon mouth and more marine-influenced; and (2) Northeast (NE; 32.9292°; 117.2461°) and (3) Southeast (SE; 32.9251°; 117.2491°) upstream stations, which are located within two different estuarine arms and are both closer to freshwater sources than the NW station. Following collection, we sieved the sediment samples using a 300 μm mesh screen to isolate macrofauna, and then used a dissecting microscope to sort identified organisms into nine taxonomic categories: Amphipoda, Copepoda, Insecta, Mollusca, Nematoda, Oligochaeta, Ostracoda, Polychaeta, and "Other." We calculated taxon composition as a percent of total specimens from each time point and averaged across the triplicates of each station. We examined the effects of the red tide (time) and location (station) on benthic macrofaunal density using two-way analysis of variance (ANOVA; alpha of 0.05). We first log-transformed the data and assessed the data for normality using a Shapiro-Wilks test (alpha of 0.05). We conducted all analyses in R version 4.1.3.

Aquarium case studies

We collected mortality data, autopsy notes, behavioral observations, and dissolved oxygen and temperature data from four aquatic facilities on the SIO campus: Hubbs Hall experimental aquarium (Hubbs), Kaplan experimental aquarium (Kaplan), the NOAA Southwest Fisheries Science Center (SWFSC) experimental aquarium, and Birch Aquarium. All four facilities were supplied with seawater from a common intake at the end of the SIO pier (depth of approximately 4 m). The initial filtration process for this intake included being gravity-fed through a pre-strainer and into a settling tank, pumped through large sand filters, and then pumped into large holding tanks before seawater was distributed to the four aquatic facilities. However, the four facilities had different secondary filtration systems. The Hubbs and Kaplan facilities lacked any additional filtration. In contrast, SWFSC had additional degassing chambers, silica sand filters, charcoal filters, fine-mesh sock filters, and

ozone and ultraviolet (UV) light sterilization. Birch Aquarium had tank-specific filtration, ranging from no additional filters to sterilization via ozone and UV light. Both SWFSC and Birch Aquarium had some tanks on recirculating aquaculture systems with <10% make-up water. Most tanks in all four facilities had some degree of supplementary aeration via bubblers or surface mixing to prevent organismal drawdown of dissolved oxygen levels.

We measured dissolved oxygen levels and temperature in each tank at SWFSC daily throughout the red tide using a HACH HQ40D portable multi meter (HACH Company, Loveland, CO, USA) and a Thermapen ONE (ThermoWorks, American Forks, UT, USA), respectively. In reaction to initial moralities at SWFSC, we began monitoring various tanks and incoming seawater for ammonia daily, starting May 3, 2020, and for pH levels intermittently, starting May 6. Total ammonia was measured with a YSI 9300 photometer and accompanying ammonia test kit (YSI, Inc., Yellow Springs, OH, USA), with unionized ammonia subsequently calculated from this value using an unionized ammonia calculator (Florida Department of Environmental Protection, 2023). The pH was calculated after a three-point calibration on a Mettler Toledo FiveEasy Plus with a LE438 pH probe (Greifensee, Switzerland), using Tris buffer standards and the USA National Bureau of Standards scale. At Hubbs we began monitoring oxygen and temperature conditions in response to organismal mortality (in select tanks at 5-minute intervals from May 1 to June 16) using a micro-oxygen sensor and temperature probe (Microx 4, Pst-7, and St26, PreSens Precision Sensing, Regensburg, Germany).

Sardine gill response

Upon the onset of red tide-induced fish mortalities within the SWFSC experimental aquarium, it became clear that fish being held at warmer temperatures were more adversely affected. In addition to collecting mortality data, we collected gill tissue samples from Pacific sardine undergoing long-term grow-out trials at 16.5°C and 19.5°C to examine potential differential responses at the blood-water interface of the gills to the red tide at different temperatures. We had previously collected gill samples from healthy, non-stressed sardine at each temperature prior to the red tide (March 18, 2020) as part of an unrelated project. We then opportunistically collected additional gill samples from moribund sardine during the red tide on May 6, 2020 (approximately 8 weeks later). We conducted all sardine gill sampling in accordance with SWFSC Animal Care and Use Committee Protocol #SW2001 (SWFSC, 2020).

We fixed sampled sardine gills in 10% formalin buffered with phosphate buffer saline (PBS) for scanning electron microscopy following methods from Wegner et al. (2013) and Kwan et al. (2019b). Briefly, we dehydrated gill samples in tert-butyl alcohol in a stepwise fashion (20% increments over 48 hours), followed by freeze-drying, and sputter-coating in gold. We imaged the gill filament and lamellar epithelium with a ThermoFisher Apreo 2 scanning electron microscope with Apero LoVac field emission gun (20 kV, 1.6 nA, 50 Pa). In total, we randomly selected

and imaged five ionocytes per fish from different gill filaments at $5000\times$ magnification. Next, we quantified the area of the apical opening of the ionocyte, as well as the number, height (h), and radius (r) of the microvilli on the apical surface, using FIJI version 2.1.0 (Schindelin et al., 2012). These measurements allowed us to estimate microvilli surface area as a cylinder ($2\pi rh$), and to calculate the total apical surface area through combination with the non-villar surface (N = 4 fish per treatment).

In addition, we fixed sardine gills in PBS-buffered 4% paraformaldehyde (12 hours) and stored them in 70% ethanol at 4°C until processing for immunohistochemistry following methods from Kwan et al. (2022). Briefly, we rinsed the fixed gill tissue samples in PBS + 0.1% Tween (PBS-T, 5 minutes), washed the samples in ice-cold PBS with sodium borohydride (1.5 mg mL^{-1}, six times, 10 minutes each), and then incubated the samples in blocking buffer (PBS-T, 0.02% normal goat serum, 0.0002% keyhole limpet hemocyanin, 1 hour) at room temperature. Next, we incubated the gill samples in blocking buffer with a primary antibody (40 ng mL^{-1}, α5 monoclonal mouse antibody, Developmental Studies Hybridoma Bank, Iowa University; Lebovitz et al., 1989) overnight at 4°C targeting Na$^+$-K$^+$-ATPase (NKA), an ion transporter found within gill ionocytes (Kwan et al., 2019b; Kwan et al., 2020; Frommel et al., 2021; Kwan et al., 2021; Montgomery et al., 2022). The next day, we washed samples in PBS-T (three times, 10 minutes each), incubated in blocking buffer with secondary antibodies (1:500, goat anti-mouse AlexaFluor^{TM} 546) and DAPI (1 μg mL^{-1}) for 1 hour, and then rinsed the samples again in PBS-T (three times, 10 minutes each) at room temperature. We mounted the gill samples onto depression slides for Z-stacked imaging on an inverted confocal microscope (Zeiss LSM 800), and then converted the images into maximum intensity projections (Zeiss ZEN 2.6 blue edition software). Next, we measured the entirety of the gill filament area pictured and counted all stained NKA-rich cells on the filament. We counted the number of NKA-rich ionocytes within each maximum intensity projection (6.4 mm^2 per image) using FIJI cell counter (plugin), and we estimated the surface areas of both the gill filament and ionocytes using FIJI freehand tool. We quantified the relative ionocyte area as the number of NKA-rich ionocytes multiplied by their average area (N = 3 per replicate), then divided by the gill filament surface area over which the ionocytes were counted, similar to the methods previously described for cutaneous ionocytes (Kwan et al., 2019a; Kwan et al., 2019b; Kwan et al., 2021). To ensure that our quantification of gill ionocytes was not biased, the tasks of imaging and blind analysis of three different filaments per fish (N = 6 fish per treatment) were performed by different researchers.

We examined the effects of temperature and red tide exposure on the number of ionocytes and relative ionocyte area using two-way ANOVA (alpha of 0.05). We assessed sardine gill microscopy datasets using the Shapiro-Wilk normality test (alpha of 0.05), which met assumptions of normality. Values are reported as mean ± SEM. We performed sardine ionocyte statistical tests using Prism (version 7.0a).

Results

Environmental dynamics

Dissolved oxygen and pH levels as recorded by various coastal and estuarine sensors throughout the duration of the red tide are shown in **Figure 3**, with the maximum and minimum values provided in **Table 1**. Estuarine sites experienced some of the most extreme hypoxia during the height and subsequent degradation of the bloom. Agua Hedionda Lagoon was intermittently hypoxic between April 29 and May 22, 2020, for a total of 186 hours (7.8 days) and completely anoxic for brief periods on April 30, May 1, and between May 11 and May 19. Los Peñasquitos Lagoon was intermittently hypoxic for a total of 420 hours (17.5 days) beginning on April 28 and continuing through May 23. The most prolonged period of hypoxia at Los Peñasquitos Lagoon occurred from May 11 to May 22, with oxygen <2 mg L^{-1} for a consecutive 254 hours (10.6 days; minimum of 0.27 mg L^{-1}, 3.65% sat; mean ± SD of 0.34 ± 0.15 mg L^{-1}, 4.93% ± 2.18% sat, N = 1019). This period appeared to be associated largely with annual Los Peñasquitos Lagoon mouth maintenance activities between May 11 and May 23, 2020, which initially involved restricting tidal flushing with the ocean and resulted in the estuary being severely hypoxic for much of this time period (minimum of 0.27 mg L^{-1}, 3.79% sat; mean ± SD of 1.04 ± 2.02 mg L^{-1}, 14.47% ± 27.54% sat, N = 1,248). Both lagoons also experienced occasional intermittent hyperoxia, with maximum values in Agua Hedionda and Los Peñasquitos Lagoons reaching approximately 16.53 mg L^{-1} (222.5% sat) and 12.16 mg L^{-1} (180.5% sat), respectively.

The near-surface inner shelf sensor at SIO pier (4 m sensor depth, 6 m bottom depth) exhibited less severe hypoxia than observed within the two monitored estuarine systems (**Figure 3B**; **Table 1**). Hypoxia occurred intermittently at the SIO sensor between April 30 and May 16, 2020, for a total of 82 hours (3.4 days). The longest consecutive period of hypoxia recorded at SIO was for 20 hours between May 4 and May 5, 2020. Hyperoxia was also observed at the SIO station, with a maximum value of 17.76 mg L^{-1} (241.9% sat).

The near-surface mid/outer shelf sites did not experience hypoxic conditions, but did experience hyperoxia. The lowest oxygen concentration observed at the Point Loma near-surface station (1 m sensor depth and 95 m bottom depth) was 7.07 mg L^{-1} (92.8% sat) while that of the South San Diego site (1 m sensor depth and 30 m bottom depth) was 5.81 mg L^{-1} (72.3% sat). Near-surface hyperoxic conditions peaked at approximately 22.49 mg L^{-1} (308.3% sat) and 23.3 mg L^{-1} (328.9% sat) at Point Loma and South San Diego, respectively, almost triple the mean percent saturation for these locations in the month prior to the bloom (108.0% ± 2.77% sat, N = 4,464, and 104.7% ± 3.0% sat, N = 4,464, for Point Loma and South San Diego, respectively). The most prolonged period of extreme hyperoxia occurred continuously for 28 days (April 21 to May 19) at the South San Diego 1 m site.

The mid-water mid/outer shelf sites (18–32 m sensor depth, 30–100 m bottom depth) did not experience hypoxia, but showed short bouts of lower oxygen (<4 mg L^{-1})

Table 1. Maximum and minimum dissolved oxygen and pH levels observed across monitoring sites during the 2020 red tide

Category[a]	Location[a]	Depth (m)		Minimum Oxygen			Maximum Oxygen			Minimum pH		Maximum pH	
		Sensor	Bottom	mg L^{-1}	% sat	Date (2020)	mg L^{-1}	% sat	Date (2020)	pH	Date (2020)	pH	Date (2020)
Estuarine	Agua Hedionda	5	6	0	0	Apr 30 / May 1 / May 11 / May 19	16.53	222.5	May 1	6.90	May 18	–[b]	–
Near-surface inner shelf	Los Peñasquitos	0.2	1.5	0.27	3.65	May 3	12.16	180.5	May 22	8.47	May 1	–	–
	SIO	4	6	0.05	0.69	May 5	17.76	241.9	Apr 23	8.79	May 9	8.67	May 18
Near-surface mid/outer shelf	Point Loma	1	95	7.07	91.82	May 20	22.49	308.3	May 1	8.00	May 21	8.88	May 1
	South San Diego	1	30	5.81	72.26	May 22	23.31	328.9	May 2	7.69	May 22	8.16	May 2
Mid-water mid/outer shelf	Del Mar	32	100	2.32	26.49	May 18	10.70	131.4	Apr 10	–	–	–	–
	South San Diego	18	30	3.73	42.25	May 21	10.21	125.4	Apr 6	–	–	–	–
Near-bottom mid/outer shelf	South San Diego	26	30	3.38	38.39	May 13	10.13	124.1	Apr 6	–	–	–	–
	LJ Canyon	29	30	1.76	19.77	May 18	4.17	47.8	May 31	–	–	–	–
	Del Mar	90	100	0.57	6.29	May 13	4.56	51.1	Apr 11	–	–	–	–
	Point Loma	89	95	2.13	23.31	Apr 1	3.88	43.0	Apr 12	7.58	Apr 3	7.78	May 7

SIO = Scripps Institution of Oceanography; LJ = La Jolla.

[a]Categories and locations as in **Figure 3**.

[b]Not available.

at later dates and at lower intensity than the estuarine and inner shelf areas (**Figure 3B**). The mid-water (18 m sensor depth) of the mid/outer shelf South San Diego site (30 m bottom depth) and the mid-water mid/outer shelf Del Mar site (32 m sensor depth, 100 m bottom depth) recorded sporadic high oxygen values up to 10.21 mg L^{-1} (125.4% sat) and 10.70 mg L^{-1} (131.4% sat), respectively, prior to the sharp decline in oxygen as the bloom decayed.

The near-bottom mid/outer shelf showed some signs of red tide-induced hypoxia and hyperoxia depending on location. For example, the near-bottom mid/outer shelf La Jolla Canyon site (29 m sensor depth, 30 m bottom depth) saw intermittent hypoxia for a total of 79 hours (3.29 days) between May 17 and May 25, 2020 (this sensor was offline between March 7 and May 11, 2020). However, the near-bottom mid/outer shelf Del Mar site (90 m sensor depth, 100 m bottom depth) only had a total of 16 hours (0.66 days) of intermittent hypoxia between April 9 and May 27, whereas the dissolved oxygen level at the near-bottom mid/outer shelf Point Loma site (89 m sensor depth, 95 m bottom depth) and South San Diego site (26 m sensor depth, 30 m bottom depth) showed reductions (<4 mg L^{-1}), but did not reach hypoxic levels. The red tide also overlapped with the onset of the spring upwelling season, and the typical upwelling signature of decreased dissolved oxygen and temperature was evident in the near-bottom mid/outer shelf sites (**Figures 3B** and S1), but dissolved oxygen concentrations generally did not reach hypoxic levels. In the near-bottom mid/outer shelf site of Del Mar (90 m sensor depth, 100 m bottom depth), the oxygen and temperature dropped from 5.02 ± 0.54 mg L^{-1} (57.1% ± 2.1% sat) and 11.62°C ± 0.66°C (N = 2,191) in January–March to 3.55 ± 0.37 mg L^{-1} (39.2% ± 4.1% sat) and 10.12°C ± 0.20°C (N = 2,571) in April–July. Similarly, at the near-bottom mid/outer shelf site of Point Loma (89 m sensor depth, 95 m bottom depth), oxygen and temperature changed from 4.11 ± 0.56 mg L^{-1} (46.4% ± 6.6% sat) and 11.41°C ± 0.66°C (N = 13,104) in January–March to 3.25 ± 0.26 mg L^{-1} (35.7% ± 2.9% sat) and 10.06°C ± 0.21°C (N = 13,104) in April–July (**Figures 3B** and S1). The near-bottom South San Diego site (26 m sensor depth, 30 m bottom depth) experienced hyperoxia up to 10.13 mg L^{-1} (124.1% sat) before dissolved oxygen levels dropped later in the bloom.

Sensors at Los Peñasquitos Lagoon, Agua Hedionda Lagoon, SIO, Point Loma, and South San Diego also monitored pH levels (**Figure 3C**). The estuarine and near-surface inner shelf sites showed unusually high pH followed by a period of abnormally low pH, which generally mirrored the dissolved oxygen profiles over the course of the bloom. Prior to the algal bloom die-off, pH levels peaked during the day at 8.79 (April 27), 8.47 (May 1), and 8.67 (May 18) at Los Peñasquitos Lagoon, Agua Hedionda Lagoon, and SIO, respectively. At night during the height of the bloom, and as the bloom began decaying, pH levels sharply decreased, with minima of 7.00 (May 9), 6.90 (May 18), and 7.06 (May 4) observed at Los Peñasquitos Lagoon, Agua Hedionda Lagoon, and SIO, respectively. Near-surface, mid/outer

shelf sites showed a consistent peak in pH throughout the bloom, with a maximum pH of 8.88 (May 1) and 8.16 (May 2) at the 1-m sensors at Point Loma and South San Diego, respectively. In contrast, pH at the near-bottom, mid/outer shelf site did not show much change from the mean value (mean ± SD: 7.70 ± 0.03, N = 9,073) during the entire red-tide period (**Table 1**).

Biological impacts
Field observations
Direct community reports and our observations showed beach strandings and mortalities of fish and invertebrates between April 29 and May 17, 2020, with the majority of mortalities occurring from May 2 to May 14 (**Figure 5**), following extreme diurnal variability and declines in oxygen (**Figure 4**, Table S2). Observed mortality spanned across 71 identified species (43 fishes, 24 invertebrates, and 4 bird species; Table S2), with demersal fishes and benthic invertebrates experiencing the highest number of mortalities (thousands of demersal fish and benthic invertebrates). Most of the observed mortalities occurred at the Agua Hedionda Lagoon, followed by the open coast sites of the Encinitas Beaches and La Jolla Beaches (**Table 2**), although reports spanned from Hollywood Beach, CA, to Ensenada, Baja California Norte, Mexico (**Figure 1**). The fish species with the highest reported mortality was the spotted sand bass (*Paralabrax maculatofasciatus*), a demersal serranid fish found in shallow, sandy environments, with hundreds of individuals recorded along Encinitas Beaches (i.e., Moonlight Beach and Grandview Beach in Encinitas, CA) and Agua Hedionda Lagoon in Carlsbad, CA, beginning on May 2, 2020. The invertebrate species with the highest reported mortality was the California bubble snail (*Bulla gouldiana*), a benthic gastropod, with hundreds of individuals found along the shores of Agua Hedionda Lagoon. In addition, several reports from divers revealed additional subtidal mortalities of species that did not wash ashore. These included topsmelt (*Atherinops affinis*), round stingray (*Urobatis halleri*), sarcastic fringehead (*Neoclinus blanchardi*), sanddabs (*Citharichthys spp.*), various rockfishes (*Sebastes spp.*), and the thornback guitarfish (*Platyrhinoidis triseriata*). Microbial mats associated with decaying organisms were observed on the coastal subtidal seafloor (at common scuba depths up to 40 m; **Figure 2D**), in shallow estuarine water (**Figure 2E**), and along the shoreline (Agua Hedionda Lagoon) in the days following the mass mortalities (**Figure 2C**). There was insufficient data to assess marine mammal mortalities in relation to the red tide due to restrictions on beach access and marine mammal stranding response during the initial months of the COVID-19 pandemic (Kerri Danil, NOAA, personal communication, 03/02/2023).

Benthic sediment macrofaunal density within Los Peñasquitos Lagoon significantly decreased during the red tide ($F_{4,30}$ = 51.866, p < 0.0001), and the recovery of macrofaunal density post-red tide differed among stations ($F_{2,30}$ = 5.357, p = 0.0103). Specifically, benthic macrofaunal densities dropped to 7.4%–13.2% of pre-red tide levels during the red tide, and by 2.5 months after the red

Figure 5. Examples of fish and invertebrate mortality during the 2020 red tide, captured by local citizens. (A, B) Images of fish kills from Agua Hedionda Lagoon in Carlsbad, CA, which had one of the highest reported fish kills on May 2, 2020, composed primarily of rock basses (*Paralabrax* spp.) and drums (various sciaenid species). Thousands of fishes (A) floated to the surface (S Anthony, May 2, 2020) and (B) subsequently washed ashore (Gary Cotter, May 3, 2020). (C) Dozens of dead *Octopus sp.* washed ashore along the rocky shore of Ensenada, Mexico (Lydia Ladah, Ensenada Center for Scientific Research and Higher Education, May 10, 2020). (D) Scavengers quickly removed carrion, like this California seagull (*Larus californicus*) with a sweet potato sea cucumber (*Molpadia arenicola*) in its beak in La Jolla, CA (Jenny Lisenbee, May 6, 2020). The extent of the mass mortality was hard to quantify in part due to these scavengers and human clean-up efforts.

tide only the NW site (closest to the ocean) had returned to pre-red tide levels, while the NE site remained at 61.5% and the SE remained at 37.6% of the pre-red tide densities (**Figure 6**). Further, macrofaunal taxon composition changed drastically with the red tide at all sites and did not return to pre-red tide composition within the 2.5 months observed following the red tide (**Figure 7**). Taxon composition differed across sites at all time points. Prior to the red tide, nematodes dominated the NW station (88.1%) and to a lesser extent the NE station (59.6%), while oligochaetes dominated the SE station (65.1%). By the end of the bloom, oligochaetes were the dominant group at the NW (76.6%) and NE (51.5%) stations, whereas at the SE station there was a more even distribution of oligochaetes

(29.2%), copepods (27.6%), ostracods (22.8%), and nematodes (18.4%). At 2.5 months following the red tide, nematodes (42.2%), copepods (27.6%), and polychaetes (22.4%) were the dominant groups at the NW site, while amphipods (29.9%), oligochaetes (28.0%), and polychaetes (24.9%) dominated the NE site, and ostracods (46.7%) and oligochaetes (24.8%) dominated the SE site (**Figure 7**). The drop in benthic macrofaunal densities and change in taxa during the red tide (May 5, 2020) were observed before estuary mouth closure (May 11 to May 23, 2020) and thus were likely driven by the red tide exclusively. However, post-red tide recovery of benthic macrofaunal densities was likely compounded by the estuary mouth closure.

Table 2. Mass mortality of fishes, invertebrates and birds resulting from the 2020 red tide

Habitat	Taxa	Ecotype	Total Species	Estimated Abundance[a]	Dates Observed (2020)	Location Code[b]
Open coast	Fishes	Demersal	16	100s	Apr 29–May 13	DM, MX, EB, SB, LJS, OB, PB, LJC, LB, HB, Dive
		Benthic	8	10s	May 5–14	MX, LJS, SB, Dive
		Pelagic	5	100s	Apr 29–May 11	LJS, Dive, SB, MB, SEB, MX, DM
	Invertebrates	Benthic	12	100s	May 3–14	BB, MX, IB, LJS, SB, NB, LJC, Dive
		In-substrate	3	100s	May 6–10	BB, LJS
		Pelagic	2	10s	May 6–10	LJS, Dive
		Sessile	2	100s	May 9–10	IB, LJS, Dive
	Birds	Semi-aquatic	1	1s	May 2	EB
		Terrestrial	1	1s	May 2	EB
Estuarine	Fishes	Demersal	15	1,000s	Apr 30–May 17	AH, Mb, LBL
		Benthic	6	100s	May 1–6	AH
		Pelagic	3	10s	May 1–6	AH
	Invertebrates	Benthic	3	100s	May 2–6	AH, LPL
		In-substrate	3	10s	May 2–6	AH, LPL
	Birds	Semi-aquatic	1	1s	May 2–6	AH
		Terrestrial	1	1s	May 2–6	AH

[a]Abundance bins of <10 (1s), 10–99 (10s), 100–999 (100s), and 1,000+ (1,000s).

[b]Location code abbreviations: Agua Hedionda Lagoon (AH), Black's Beach and Torrey Pines State Beach (BB), Del Mar Beaches and San Dieguito River Mouth (DM), Encinitas Beaches (EB), Ensenada, Mexico (MX), Hollywood Beach (HB), Imperial Beach (IB), La Jolla Cove (LJC), La Jolla Canyon (Dive), La Jolla Shores and Scripps Beach (LJS), Long Beach (LB), Los Peñasquitos Lagoon (LPL), Los Batiquitos Lagoon (LBL), Mission Bay (Mb), Mission Beach (MB), Newport Beach (NB), Oceanside Beach (OB), Pacific Beach and Tourmaline (PB), San Elijo State Beach (SEB), and Solana Beach (SB). See **Figure 1** for map locations.

Aquarium case studies

Unlike field sites, dissolved oxygen and pH levels were not monitored continuously at the Hubbs, Kaplan, and Birch aquarium facilities fed by the SIO pier seawater intake. However, spot sampling began after red tide-induced mortalities began, which showed that dissolved oxygen levels dropped to 0 mg L^{-1} (0% sat) in numerous tanks on May 5, 2020 (Figure S2). At the SWFSC experimental aquarium, daily sampled dissolved oxygen levels never dropped below 6.3 mg L^{-1} (84% sat) in any of the tanks (Figure S2). Likewise, spot checking various tanks at the Birch Aquarium from May 1 to May 16 did not show signs of hypoxia (dissolved oxygen only dipped below 70% sat on three occasions, each in a separate tank).

Opportunistic pH measurements at the SWFSC experimental aquarium showed pH levels similar to those observed at the SIO pier sensor (**Figure 3C**). During the measurement period from May 3 to May 14, 2020, pH was lower than normal (typically at 8.00) and variable across twelve tanks with flow-through water (mean ± SEM of 7.80 ± 0.03, N = 40) with a low pH of 7.41 on May 7 and a maximum pH of 8.13 on May 10. Spot checks of total ammonia levels at the SWFSC following initial fish mortalities showed elevated concentrations in the incoming seawater (mean ± SEM of 0.22 ± 0.04 mg L^{-1} N, 0.0042 ± 0.0007 mg L^{-1} unionized NH_3, N = 13) from May 6 to May 20, across eleven flow-through tanks (0.28 ± 0.02 mg L^{-1} N, 0.0048 ± 0.0004 mg L^{-1} unionized NH_3, N = 67) from May 3 to May 20, and across five recirculating aquaculture system tanks (0.33 ± 0.06 mg L^{-1} N, 0.0051 ± 0.0011 mg L^{-1} unionized NH_3, N = 13) from May 6 to May 20. The maximum observed total ammonia concentration was 0.82 mg L^{-1} N, which occurred in both a flow-through tank and a RAS tank on May 6, and maximum unionized ammonia concentration was 0.0167 mg L^{-1} NH_3 on May 6 in a flow-through tank. Ammonia soon returned to normal in all tanks (sustained levels < 0.1 mg L^{-1} N) after May 20. For intervention purposes, 1 L of AmQuel Plus ammonia detoxifier (Kordon LLC, CA, USA) was added to the RAS following the daily ammonia checks from May 6 to May 9 to lower the ammonia levels.

Red tide-induced mortalities occurred in all four aquariums (**Table 3**), but Kaplan and Hubbs aquariums experienced higher mortalities in their flow-through animal holding tanks (81% and 48%, respectively) than those at the SWFSC aquarium (26%) and Birch Aquarium (<1%), both of which did not experience hypoxic conditions. In addition to mortality differences across aquariums, certain species appeared to be affected disproportionately. For
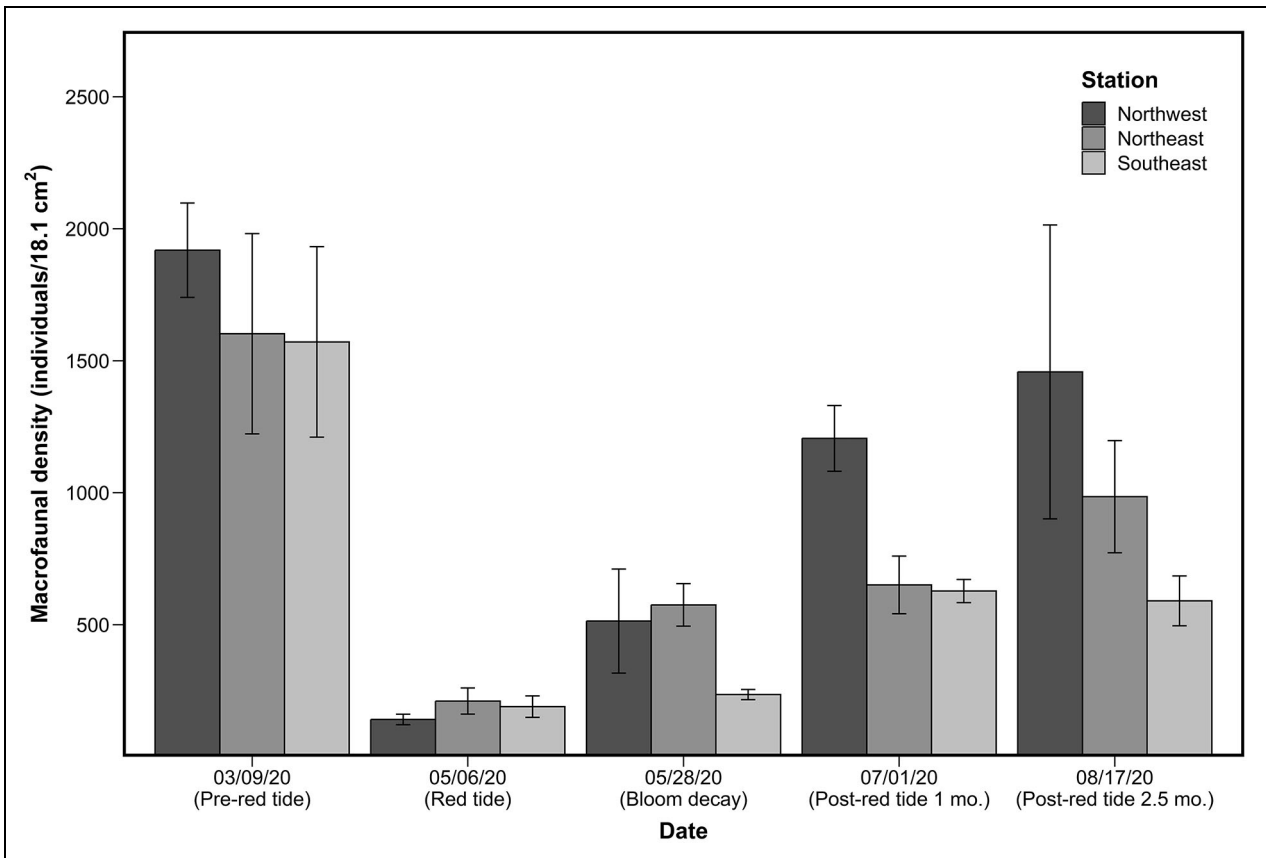
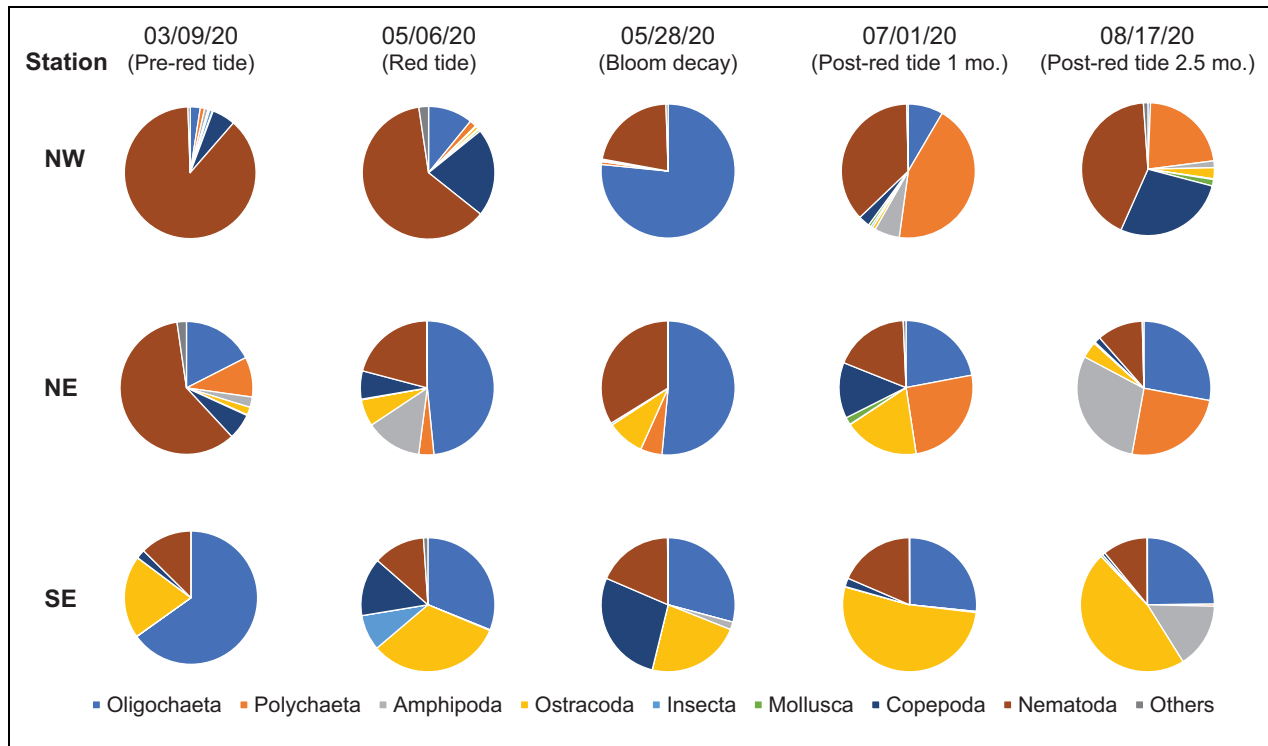**Figure 6. Red tide-induced changes in benthic macrofaunal densities at Los Peñasquitos Lagoon**. Benthic soft-sediment macrofaunal (>300 μm) invertebrate densities (mean ± SEM) calculated as number of individuals at 0–5 cm depth in 18.1 cm² sampling cores within Los Peñasquitos Lagoon, California, USA, at various time points pre-, during, and post-red tide at three separate stations: Northwest (station closest to the mouth of the lagoon and ocean), Northeast (station farther inland), and Southeast (station located farthest inland closest to the freshwater sources). Annual lagoon mouth closure (May 11 to May 23, 2020) occurred after the first two sampling time points and reopened prior to the last three sampling time points. Dates are month/day/year.

instance, 100% of splitnose rockfish (*Sebastes diploproa*; 63 individuals) at Hubbs aquarium and various other rock-fishes (15 of 20 individuals comprising five species; 50%–100% depending on species) at SWFSC aquarium died. In contrast, only 2.2% of white seabass (*Atractoscion nobilis*; 1 individual) at Hubbs, 12.5% of horn sharks (*Heterodontus francisci*; 1 individual) at Kaplan aquarium, and 27.8% of Pacific sardine (291 individuals) in the SWFSC aquarium perished during the red tide. Similarly, there was high observed mortality in certain invertebrate species such as 90% mortality of California mussel (*Mytilus californianus*; 90 individuals) in Kaplan aquarium, 78% of Pacific oysters (*Magallana gigas*; 18 individuals) and 71.4% of painted sea urchin (*Lytechinus pictus*; 75 individuals) in Hubbs aquarium, while there was only 30% mortality of purple sea urchins (*Strongylocentrotus purpuratus*; 92 individuals) in Hubbs aquarium, and only 4.5% mortality of black abalone (*Haliotis cracherodii*; 1 individual), and 1.7% mortality of white abalone (*Haliotis sorenseni*; 2 individuals) in flow-through tanks in the SWFSC aquarium. There was lower mortality reported from the Birch Aquarium, but reports of mortalities began on April 10, 2020, closer to the onset of the bloom, than in Kaplan aquarium

(April 27) and Hubbs and SWFSC aquariums (both May 2). There were no observed mortalities associated with the red tide in the recirculating systems at SWFSC aquarium nor the Birch Aquarium. Finally, Pacific sardine reared at 19.5°C experienced higher mortalities (59.3%) than those reared at lower temperatures (13.5°C and 16.5°C; 17.7% and 17.6%, respectively), thereby suggesting warmer temperature may have been an additive stress that exacerbated the effects of the red tide for this species (Table S3).

In addition to direct mortality, we also noted marked behavioral and sublethal health changes in various aquarium animals associated with the red tide. During the height of the red tide, fish were visibly agitated as seen through increased activity, spy-hopping, and mouthing near the surface at all facilities. At SWFSC, some rockfish and sardine were noted breaching the surface, with some jumping out of the tank entirely. In addition, many animals stopped feeding during the height and latter stages of the red tide and in some cases (e.g., two cowcod, *Sebastes levis*, and one sunset rockfish, *Sebastes crocotulus*) never regained their appetite, which led to emaciation and eventual death several months later (the last of the three rockfish was euthanized on November 24, 2020, due to

Figure 7. Red tide-induced changes in benthic macrofaunal taxon composition at Los Peñasquitos Lagoon. Benthic soft-sediment macrofaunal (>300 μm) taxon composition (%) within Los Peñasquitos Lagoon, California, USA at various time points pre-, during, and post-red tide at three separate stations: Northwest (NW, station is located closest to the mouth of the lagoon and ocean), the Northeast (NE, station is further inland), and the Southeast (SE, station is located furthest inland closest to the freshwater sources). Annual lagoon mouth closure (May 11 to May 23, 2020) occurred after the first two sampling time points and reopened prior to the last three sampling time points. Dates are month/day/year.

emaciation). The red tide also appeared to have compromised the immune systems for some individuals. For example, autopsies at the Birch aquarium found protozoans on the gills of a native spotted kelpfish (*Gibbonsia elegans*) and non-native southern crested weedfish (*Cristiceps australis*) housed in separate tanks. Likewise, several aquarium animals exhibited secondary infections that started during or shortly after the red tide; for example, one surviving cowcod (*Sebastes levis*) had an eye infection that began during the red tide and persisted for almost 2 years.

Sardine gill response

Scanning electron microscopy and immunohistochemistry analyses were conducted on the gills of Pacific sardine undergoing long-term grow-out trials at 16.5°C and 19.5°C at SWFSC aquarium in order to understand the effects of the red tide on gill physiology. These fish were not exposed to hypoxia during the red tide but experienced different rates of mortality with temperature (Table S3). Scanning electron microscopy analyses did not show any obvious signs of mechanical damage to the gill epithelium induced by the red tide (**Figure 8A**). The mean apical pit surface area of gill ionocytes was significantly increased in response to the red tide ($F_{1,12} = 30.320$, p = 0.0001; two-way ANOVA), but not significantly affected by temperature ($F_{1,12} = 1.777$, p = 0.2072; **Figure 8B**). When the microvillar area was included, the surface area of the

sardine gill ionocyte apical pit was significantly greater for sardine exposed to both the red tide ($F_{1,12} = 18.280$, p = 0.0011) and warmer temperature ($F_{1,12} = 10.050$, p = 0.0081; two-way ANOVA; **Figure 8C**). In both cases, there was no significant interaction effect between red tide and temperature on apical pit surface area ($F_{1,12} = 0.045$, p = 0.8363) or between microvilli and apical pit surface area ($F_{1,12} = 4.198$, p = 0.0630).

Immunohistochemistry analyses did not show any significant difference in ionocyte localization (**Figure 9A**). The number of ionocytes in sardine gills was not significantly affected by temperature ($F_{1,20} = 2.975$, p = 0.1000) or red tide exposure ($F_{1,20} = 0.618$, p = 0.4409; two-way ANOVA; **Figure 9B**). However, relative ionocyte area was significantly lower in the warmer temperature treatment ($F_{1,20} = 10.740$, p = 0.0038), but remained unaffected by red tide exposure ($F_{1,20} = 1.110$, p = 0.3046; two-way ANOVA; **Figure 9C**). In both cases, there was no significant interaction effect in the number of ionocytes ($F_{1,20} = 2.636$, p = 0.1202) or relative ionocyte area ($F_{1,20} = 3.794$, p = 0.0656).

Discussion

The 2020 red tide was one of the longest and most intense harmful algal blooms ever recorded off the coast of southern California and resulted in both acute and prolonged changes in water quality that had extensive negative impacts on both coastal ecosystems and within local

Table 3. Fish and invertebrate mortality at four aquarium facilities that utilized flow-through seawater during the 2020 red tide

Aquarium	Common Name	Scientific Name	Date Range (2020)[a]	Total Mortality	Mortality (%)[b]
Hubbs	Splitnose rockfish	*Sebastes diploproa*	May 2	63	100
	Swell shark	*Cephaloscyllium ventriosum*	May 2	9	100
	Treefish	*Sebastes serriceps*	May 2	4	80
	Round stingray	*Urobatis halleri*	May 2	2	22
	White seabass	*Atractoscion nobilis*	May 2	1	2.2
	Pacific oyster	*Magallana gigas*	May 6–10	18	78
	Dwarf cuttlefish[c]	*Sepia bandensis*	NR[d]	10	100
	Painted sea urchin	*Lytechinus pictus*	NR	75	71.4
	Purple sea urchin	*Strongylocentrotus pupuratus*	NR	92	30
Kaplan	Yellowfin goby	*Acanthogobius flavimanus*	Apr 27–May 10	2	100
	Sarcastic fringehead	*Neoclinus blanchardi*	May 1–4	2	100
	Longjaw mudsucker	*Gillichthys mirabilis*	May 4–7	4	40
	Horn shark	*Heterodontus francisci*	May 1	1	12.5
	Shovelnose guitarfish	*Pseudobatos productus*	NR	1	100
	California mussel	*Mytilus claifornianus*	NR	90	90
SWFSC	Sunset rockfish	*Sebastes crocotulus*	May 6–Nov 24	7	87.5
	Cowcod	*Sebastes levis*	May 6–Nov 4	5	62.5
	Rosy rockfish	*Sebastes rosaceous*	NR	1	50
	Yellowtail rockfish	*Sebastes ruberrimus*	NR	1	100
	Copper rockfish	*Sebastes caurinus*	NR	1	100
	Pacific sardine	*Sardinops sagax*	May 2–14	291	27.8
	Black Abalone	*Haliotis cracherodii*	May 14	1	4.5
	White Abalone	*Haliotis sorenseni*	Apr 27–Jun 8	2	1.7
Birch Aquarium	Pacific seahorse	*Hippocampus kuda*	Apr 10–Jun 28	13	NR
	Dwarf seahorse[c]	*Hippocampus zosterae*	Apr 22–Jun 1	3	NR
	Barbour's seahorse[c]	*Hippocampus barbouri*	Apr 24–Jun 30	4	NR
	Pot-bellied seahorse[c]	*Hippocampus abdominalis*	May 5–Jun 30	4	NR
	Northern seahorse[c]	*Hippocampus erectus*	Apr 17–Jun 30	3	NR
	Crystal jelly	*Aequorea victoria*	May 17	Multiple	NR
	California seahare	*Aplysia californica*	May 2–19	2	NR
	Southern crested weedfish[c]	*Cristiceps australis*	May 6–Jul 1	2	NR
	Treefish	*Sebastes serriceps*	May 7	1	NR
	Spotted kelpfish	*Gibbonsia elegans*	May 9	1	NR
	Vermillion rockfish	*Sebastes miniatus*	May 13	1	NR
	Copper rockfish	*Sebastes caurinus*	May 13	1	NR
	California spiny lobster	*Panulirus interruptus*	May 25	1	NR
	Staghorn coral colony[c]	*Acropora sp.*	Jun 12	2	NR
	Thin birdsnest coral colony[c]	*Seriatopora hystrix*	Jun 12	2	NR

(continued)

Table 3. *(continued)*

Aquarium	Common Name	Scientific Name	Date Range (2020)[a]	Total Mortality	Mortality (%)[b]
	Cactus coral[c]	*Pavona decussata*	Jun 12	1	NR
	Gray smoothhound	*Mustelus californicus*	Jul 1	1	NR

[a]Date range indicates the first reported mortality and last reported mortality for each species. Some fish stopped eating during/after the red tide and died upward of 6 months later.

[b]Percent mortality was not recorded (NR) for the Birch Aquarium, which exhibited low mortality rates.

[c]Species not native to Southern California.

[d]Not recorded.

aquarium facilities. Based on water pigmentation, filtration difficulty, and microbial community composition, Wilson et al. (2022) classified the red tide into periods of bloom (April 1 to May 18, 2020) and post-bloom (i.e., bloom decay; May 19 to June 4, 2020) with the highest phytoplankton concentrations (above 10^6 cells L^{-1}) observed from April 20 to May 11 and reaching a peak on April 30. Our environmental and biological observations follow this timeline closely, with the growth and decay of the bloom resulting in drastic changes in dissolved oxygen and pH which were exacerbated within the estuarine and inner shelf (near-shore coastal) environments. Mass fish and invertebrate die-offs occurred during and shortly after the peak of the bloom and were associated with low oxygen levels, variable pH, and potentially other factors such as chemical byproducts produced by the bloom and its subsequent breakdown. While changes to single physical environmental factors (e.g., oxygen, pH) can cause physiological stress and mortality to marine organisms, this red tide event was particularly detrimental in that there were multiple and compounding changes to environmental parameters that were both intense and sustained over days to weeks. Here, we discuss the effects of this historic red tide on various water parameters and observed effects on animal health and physiology, with some comments on potential future mitigation strategies.

Environmental dynamics

Local environmental conditions during the red tide were closely linked with bloom dynamics over both acute (e.g., diel patterns in photosynthetic activity and respiration) and prolonged (i.e., bloom growth and decay) time scales. The beginning of the red tide was indicated by a marked increase in cell counts of *Lingulodinium polyedra* offshore on March 31, 2020, but widespread acute changes to coastal environmental oxygen levels and pH largely did not appear until approximately 10 days later, around April 10. Clear diel patterns in both dissolved oxygen and pH occurred across all sites, reflecting phytoplankton photosynthesis during the day and organismal respiration at night (**Figure 4**; Hitchcock et al., 2014; Hirsh et al., 2020). During the day, *L. polyedra* and other primary producers removed dissolved carbon dioxide from the water

and produced oxygen as a byproduct during photosynthesis that led to large increases in both dissolved oxygen levels (hyperoxia) and pH. At night, collective bloom and community respiration led to sharply reduced environmental oxygen (often reaching hypoxic or even anoxic levels) and marked increases in carbon dioxide that decreased environmental pH.

As in past red tide observations (Marasovic et al., 1991; Cai et al., 2011; Hofmann et al., 2011), the variation in dissolved oxygen and pH reflected bloom intensity and showed distinct temporal and spatial patterns associated with bloom development and decay. During April and early May 2020, the increased primary productivity resulted in sustained periods of daily hyperoxia and increased pH during daylight hours in the estuarine, inner shelf, and near-surface and mid-water mid/outer shelf environments. The most extreme hyperoxia (>200% sat) and pH (>8.5) occurred in the estuarine and near-surface environments where the bloom was mainly concentrated. Mean pH values generally increased during April and early May as the density of phytoplankton increased and collectively removed more carbon dioxide for primary production. During the same period (end of April and for the first 2 weeks of May), there was sustained nighttime and more severe hypoxia in the estuarine and inner shelf environments. Ultimately, as the red tide began to decay in mid to late May (as noted by the sulfuric smell, protein foam deposits, microbial matting, and drastic decline in cell counts of *Lingulodinium polyedra*), there were sustained periods of subsurface hypoxia and low pH during both daylight and nighttime hours in the estuaries, inner-shelf coastal, and to a lesser extent, some near-bottom mid/outer shelf sites. While the near-bottom mid/outer shelf environment exhibited sporadic hypoxia and lower pH across the bloom associated with the red tide, oxygen concentrations and pH remained relatively consistent and were likely buffered by stratification and circulation at these sites or possibly by deeper upwelled water.

Although the estuarine environment is naturally characterized by occasional periods of hypoxia and near-anoxia during times of low flow and mixing (Nezlin et al., 2009; Levin et al., 2022), the red tide led to multiple anoxic events within the estuarine environment, and the shallow
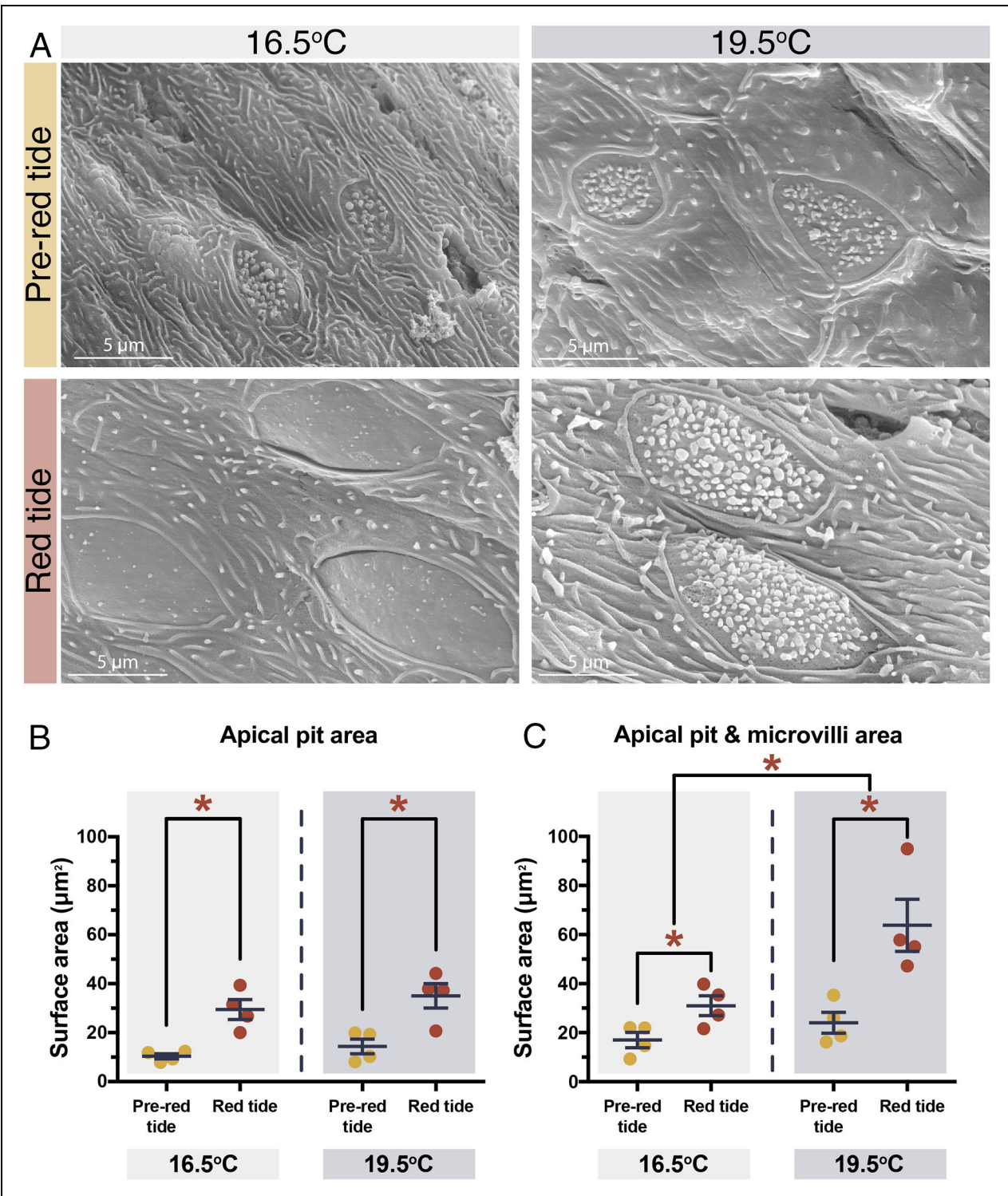
Figure 8. Scanning electron microscope analyses of the apical surface of Pacific sardine gill ionocytes. (A) Representative images of ionocyte apical morphology before and during red tide exposure at 16.5°C and 19.5°C. (B) Mean ionocyte apical pit area before and during red tide exposure at 16.5°C and 19.5°C. (C) Mean ionocyte apical pit area including the surface area of the microvilli before and during red tide exposure at 16.5°C and 19.5°C. Error bars in (B) and (C) indicate SEM. Asterisks denote statistically significant differences ($\alpha = 0.05$).

inner shelf experienced abnormally low oxygen levels, reaching near anoxia (**Table 1**). These decreases in dissolved oxygen were accompanied by increases in carbon dioxide with extreme pH values approaching 6.9 in the estuaries and inner shelf. While acute low oxygen and pH events do occur in shallow water along the coasts of southern California and northern Baja California with strong upwelling events and occasional strong red tides, to our knowledge such extended periods of low oxygen (down to 0.05 mg L^{-1}) and pH (down to 7.06) in the inner shelf environment have not been reported previously (Frieder et al., 2012; Low et al., 2021; Kekuewa
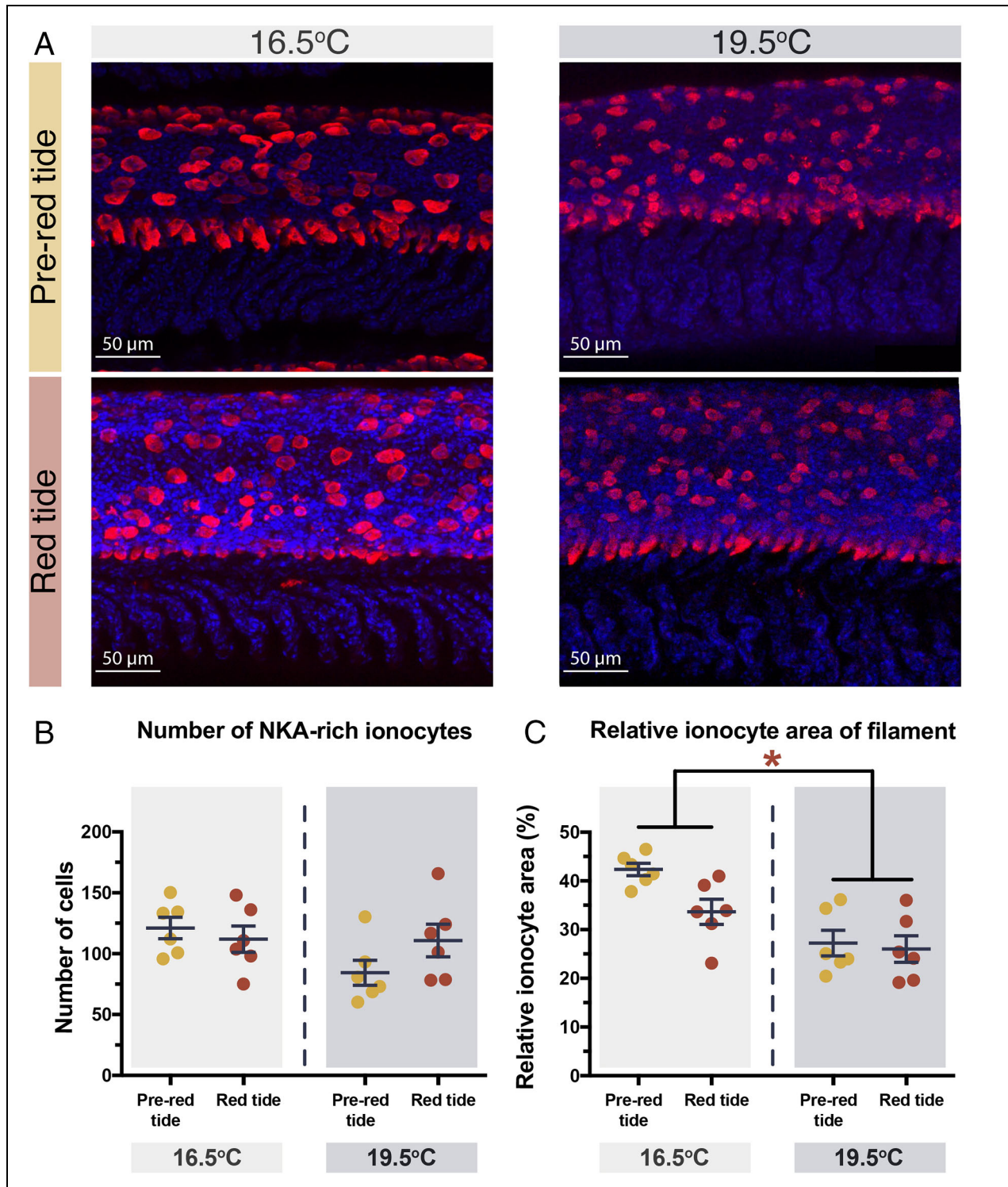
Figure 9. Immunohistochemistry analyses of sardine gill ionocytes. (A) Representative images of ionocytes, rich in the ion transporter Na^+-K^+-ATPase (NKA, stained pink), located on the gill filaments before and during the red tide at 16.5°C and 19.5°C. (B) Number of ionocytes before and during the red tide and at 16.5°C and 19.5°C. (C) Relative ionocyte area (% coverage of gill ionocytes on the gill filament) before and during the red tide at 16.5°C and 19.5°C. Error bars in (B) and (C) indicate SEM. Asterisk denotes a statistically significant difference ($\alpha = 0.05$).

et al., 2022; Wilson et al., 2022; open access data via Scripps Ocean Acidification Real-time [SOAR] Monitoring Program, 2023). For example, autonomous measurements of oxygen and pH off Scripps pier (SOAR program) that began in 2018 and 2012, respectively, allow for direct comparison to a more typical phytoplankton bloom that occurred during the spring of 2023, which led to a much more modest decrease in oxygen (minimum of 4.31 mg L^{-1} on April 30, 2023) and pH (minimum of 7.70 on April 30, 2023) that did not show corresponding harmful impacts on the local fish and invertebrate community (SOAR, 2023).

Biological impacts
Field observations

Although reports of dead marine organisms were sporadic across the duration and range of the bloom, mass mortality events were highly concentrated in time and space. The highest reported mortality occurred between May 2 and May 6, 2020, which overlapped and shortly followed the peak of the bloom and corresponded with longer and more intense daily hypoxia and low pH (**Figures 3** and **4**), as well as increased concentrations of sulfur compounds including several volatile compounds (E. Ternon and J. Dinasquet, unpublished data). Mass mortality was disproportionately reported from the La Jolla area (encompassing La Jolla Cove, La Jolla Shores Beach, and Scripps Beach), Encinitas area, and Agua Hedionda Lagoon. These areas seemed to experience the highest bloom density and most adverse environmental conditions based on our sensor data, and in comparison to reports from other locations; for example, *Lingulodinium polyedra* density was much higher at the SIO pier than when sampled at the same time off the Santa Monica pier (Kahru et al., 2021). Although the Encinitas area is largely exposed open coast, the other locations (i.e., La Jolla area, lagoons) are partially or nearly completely enclosed or protected areas, which can impede mixing and increase physical retention conducive to bloom formation and trapping (e.g., Pitcher et al., 2010). For example, the southern end of the La Jolla area is composed of a partially protected cove, and much of La Jolla Shores beach experiences reduced wave action due to refraction and diffraction effects of waves off the head of the La Jolla submarine canyon (Munk and Traylor, 1947; Magne et al., 2007; Nosal et al., 2013). In addition to concentrating *L. polyedra* density and potentially enhancing bloom dynamics through local upwelling associated with the canyon (Hickey, 1995; Allen et al., 2001), the impediment of wave action and flow dynamics may have also allowed for the concentration of detritus and carcasses in this region. The La Jolla area also contains two marine protected areas (Matlahuayl State Marine Reserve and San Diego-Scripps Coastal State Marine Conservation Area). Generally, marine protected areas have higher biomass, density, and species richness of organisms compared to non-protected areas (Starr et al., 2015), which may have contributed to the high mortality observed. Finally, frequent foot traffic in the La Jolla and Encinitas area may have resulted in higher mortality reports relative to other locations. Interestingly, larger estuaries such as Mission Bay and San Diego Bay appeared less impacted by the red tide, which likely reflects the patchy nature of red tides and influence of other local processes on bloom proliferation (e.g., embayment mixing). In fact, the San Diego State University Coastal and Marine Institute Laboratory, which uses flow-through seawater from San Diego Bay, did not experience any adverse effects during the red tide (L. Miller, personal communication, 17/03/2023).

The red tide affected species across ecotypes, but nearshore demersal species comprised the largest proportion of observed mortality. For many of these nearshore demersal species, the red tide encompassed much of the surrounding viable habitat, which likely prevented the organisms from escaping extreme conditions. Specifically, many benthic and demersal species tend to be less mobile and exhibit strong site fidelity and are thus less likely to leave their preferred habitat while experiencing stressful conditions (Green et al., 2011; Hannah and Rankin, 2011; Rankin et al., 2013; Harding et al., 2019) until it is too late to travel the large distances required to escape. Such situations are exacerbated in lagoons where conditions can deteriorate quickly and animals may have trouble locating potentially less intense conditions on the open coast. In contrast, more active species generally exhibit higher mobility, which likely helps them actively avoid suboptimal conditions. Gannon et al. (2009) found that the biomass of planktivorous pelagic fishes, like clupeids, actually increased during phytoplankton blooms of *Karenia brevis* to take advantage of additional food, while also indicating these species have either a higher tolerance of suboptimal conditions or the ability to detect and avoid them. However, while they comprised a low proportion of total mortality, there were still some instances of mortality in pelagic species, including the shortfin mako (*Isurus oxyrinchus*) and Pacific chub mackerel (*Scomber japonicas*). While such species should easily be able to avoid the red tide, the conditions in certain areas were likely so deteriorated that even acute accidental exposure resulted in disorientation and mortality. Also, our observations of organismal mortality were based primarily on beach wash-ups; thus, mortality of negatively buoyant, pelagic, and deeper-dwelling fishes are all likely heavily underreported. Additionally, scavengers quickly removed/consumed dead organisms (**Figure 5D**), which likely led to further under-reporting of mortality.

In addition to large scale mortality events observed for larger fishes and invertebrates, ongoing field work at the Los Peñasquitos Lagoon allowed for unique insight into the effects of the red tide on smaller sessile and in-substrate species which usually go unquantified. Soft-sediment macrofauna invertebrate densities within the Los Peñasquitos Lagoon crashed, dropping to 7.4%–13.2% of pre-red tide levels depending on sampling site. Likewise, benthic macrofaunal invertebrate diversity and species composition saw marked shifts, presumably reflecting taxa more resilient to hypoxia and other adverse conditions. While all sampling sites within the lagoon saw drastic changes, sampling sites differed in species composition and rates of recovery, testifying to the patchy and location-specific responses to the red tide, even within a single estuary. Of note was the faster recovery of species density at the sampling site closest to the ocean, which after 2.5 months saw macrofaunal densities similar to those before the red tide, although community composition still differed. The slower recovery by the inner estuary sites suggests protracted post-red tide effects for much of the estuary that are likely to affect fish and invertebrate recruitment (Flaherty and Landsberg, 2011). These spatial effects are likely explained by increased residency times of bloom dynamics and decreased ocean flushing of the inner estuary to help reseed affected areas. Considering this lagoon undergoes annual mouth maintenance, which can affect ocean flushing and thus influence benthic

macrofaunal recovery (Levin et al., 2022; Neira et al., 2022), our results suggest that such maintenance activities might need to consider potential complications associated with red tides.

Despite widespread mortality of many nearshore and estuarine taxa, there were some communities that appeared to escape the red tide relatively unscathed. For example, we did not observe high mortality rates for open-coast intertidal species. While low mortality rates could represent sampling bias as these species are generally small and cryptobenthic, such species typically experience more extreme daily and seasonal environmental conditions associated with tidepool isolation and aerial exposure and are thus generally tolerant to acute and extreme changes in oxygen, pH, temperature, salinity, and ammonia levels (Diaz et al., 1995; Richards, 2011) and thus likely better adapted to survive the prolonged environmental stressors caused by red tides. Similarly, there was no evidence of changes in the density or growth rates of giant kelp (*Macrocystis pyrifera*), stalked kelp (*Pterygophora californica*), and *Laminaria farlowii* or changes in the density or size structure of La Jolla and Point Loma kelp forests (long-term data from seven sites; Dayton et al., 1999; Parnell et al., 2020; Parnell et al., 2022), despite there being little to no light transmittance measured by sensors at both La Jolla (24 m depth) and Point Loma (depths: 9 m, 15 m, 24 m) during the red tide (E. Parnell, unpublished data). In contrast, a nearby sensor located at the edge of La Jolla Canyon with no kelp present recorded a prolonged period of hypoxia during the bloom decay, with evidence of demersal fish mortality (**Figure 3**, **Table 1**). Such examples suggest the resiliency of certain communities to the effects of the red tide, and that specific mechanisms (e.g., kelp forest productivity) potentially buffering against adverse water conditions, deserve further study.

Aquarium case studies

The timing and extent of mortality within local aquarium facilities appeared to closely mirror mortality in the wild, with most aquarium mortality occurring on or around May 2, 2020, and the following week. Mortality in the Hubbs and Kaplan aquaria appeared to be associated with acute hypoxia and anoxia exposure from the incoming water being drawn from the end of the SIO pier. However, simultaneous mass mortality events also occurred in the SWFSC aquarium, even though dissolved oxygen levels in all animal holding tanks always remained >80% sat due to ozone (O_3) sterilization which artificially oxygenates the water (O_3 degrades into O_2). Based on fish behavioral observations, we hypothesize that mortality in these fishes was caused by lethal levels of nitrogenous or sulfuric compounds associated with the bloom and its breakdown within the aquarium water, which may have had synergistic impacts on fish already stressed by increased variability in pH/CO_2. For example, we observed rockfishes and sardine in the SWFSC experimental aquarium attempting to jump out of their tanks (some successfully) in what appeared to be an attempt to avoid lethal water conditions, despite tank dissolved oxygen levels near 100%

saturation. Upon observation of this behavior, we greatly increased aeration to the tanks, which appeared to quickly limit the behavior, indicating that the increased aeration may have helped to off-gas nitrogenous and sulfuric compounds from the water and possibly stabilize pH/CO_2. In addition, sardine housed in the SWFSC aquarium showed red irritation around the eyes and snout consistent with excess chemical exposure to ammonia or hydrogen sulfide (Roberts and Palmeiro, 2008).

While ammonia, other nitrogenous compounds (i.e., nitrate and nitrite), and hydrogen sulfide were not being monitored at the time of mass mortality, post-sampling at SWFSC showed elevated levels of both total ammonia (>0.1 mg L^{-1} N; maximum of 0.82 mg L^{-1} N) and unionized ammonia (maximum of 0.0167 mg L^{-1} NH$_3$) for 2 weeks following initial mortality. Although unionized ammonia levels measured post-mortality at SWFSC were generally below established sublethal toxicity thresholds for marine organisms (>0.0125–0.05 mg L^{-1} NH$_3$; Timmons and Ebling, 2010; Becke et al., 2019), there were no measurements available from the height of mass mortality from any of our facilities or from the wild. Considering the broad daily fluctuations in temperature and pH across all sites, ammonia levels also likely changed drastically across acute time scales and locations. Likewise, sulfur reactions were likely prevalent at this stage of the red tide (Shipley et al., 2022), and preliminary measurements indicate a variety of dissolved sulfur compounds were present along the coast during the height of the red tide (E. Ternon, unpublished data). Both unionized ammonia and hydrogen sulfide are known to have negative effects on fish health, both individually and compounded with low dissolved oxygen and high pH (Bagarinao and Lantin-Olaguer, 1998; Boardman et al., 2004; Santhosh and Singh, 2007; Bhatnagar and Devi, 2013; Franklin and Edward, 2019). In comparison, the Birch Aquarium did not exhibit high rates of organismal mortality, which may be attributed to larger volume tanks with higher mixing and aeration, limiting both oxygen depletion as well as buildup of other compounds. Additionally, mortality did not occur in the SWFSC or Birch Aquarium recirculating aquaculture systems, which were only receiving a small percentage (<10%) of makeup water from the SIO pier.

Our combined field and aquarium observations suggest that, in most cases, the immediate contributing factor to mortality was acute exposure to extreme hypoxia. However, increased ammonia and other nitrogenous compounds, sulfuric byproducts, and variable pH levels, also likely had additive and/or compounding effects that contributed to further stress and mortality. In rare cases, such as in some seahorses at the Birch Aquarium, high mortality rates were attributed to an increase in suspended solids that clogged gills. While *Lingulodinium polyedra* is known to produce yessotoxin, which can have adverse effects on organisms (Armstrong and Kudela, 2006; Howard et al., 2008; De Wit et al., 2014; Pitcher et al, 2019), yessotoxin was only detected in low concentrations in water samples (range of 0.27–1.89 ng L^{-1}) and particle samples (range of nd–2.80 ng L^{-1}) collected off the SIO pier from April 24 to May 6, 2020 (Ternon et al., 2023) and in particle samples

and bivalve tissue samples collected during the height of the bloom from coastal waters off Ensenada, Mexico (E. Garcia-Mendoza, Ensenada Center for Scientific Research and Higher Education, personal communication, 09/02/2023). While species-specific responses to yessotoxin are widely unknown, we believe these levels are generally too low to cause organismal mortality compared to levels detected from other mass mortality events (De Wit et al., 2014; Pitcher et al, 2019). However, the cumulative effects of altered water quality in addition to some potentially low levels of bloom toxicity associated with yessotoxin or from other HAB byproducts require further study.

In addition to succumbing directly to adverse water conditions, we saw evidence that red tide-induced physiological stress potentially compromised animal immune system function and led to other health issues. For animals that survived the red tide exposure, many showed lasting effects. For example, the health of multiple rockfish individuals at the SWFSC aquarium declined over time and led to their death upward of 6 months post-red tide. As of November 2023 (3.5 years post-red tide) several rockfishes exposed to the red tide still exhibit increased incidences of bacterial infection as well as general lethargy and slow response to food and other stimuli in comparison to fish that were collected following the red tide, suggesting some permanent health or fitness effects from red tide exposure. Such observations are consistent with other harmful algal blooms that have been shown to alter activity level and behavior in dolphins (McHugh et al., 2010), crabs (Gravinese et al., 2020), and fishes (Hallegraeff, 2003), including loss of appetite (Landseberg, 2002). Changes to environmental conditions could also potentially affect long-term reproductive fitness (e.g., spawning behavior, gonad development, egg quality) and, ultimately, success of progeny (Coutant, 1987; Schreck et al., 2001; Schreck, 2010; Mileva et al., 2011; Fennie et al., 2023).

Sardine gill response

Ongoing research on Pacific sardine begun prior to the red tide allowed us to assess potential gill damage and the gill physiological response to the adverse water conditions. Given the filtration systems at the SWFSC aquarium, sardine were spared from hypoxia, but were chronically exposed to low pH along with exposure to high levels of ammonia and suspected sulfuric compounds. Unlike some species at the Birch Aquarium, the gills of Pacific sardine were not physically clogged nor physically damaged, despite redness to the snouts and eyes attributed to chemical exposure. However, exposure to the red tide did appear to increase the apical surface area of existing gill ionocytes, which increased further at warmer temperature. This apparent red tide effect suggests an elevated demand for ion-transport, consistent with increased demands for internal acid-base balance associated with suboptimal environmental pH/CO_2 and hyperammonemia. In addition, exposure to warmer temperature might have increased the rates of metabolically produced NH_4^+ and H^+ ions, requiring a larger apical surface area in existing gill ionocytes to facilitate their excretion and

potentially increasing energetic demands leading to higher mortality. However, sardine did not appear to synthesize additional gill ionocytes to cope with red tide exposure, which is a potentially longer and more energetically expensive investment involving the proliferation of these specialized cells (Kreiss et al., 2015). Ionocyte synthesis in response to elevated environmental CO_2 levels has only been reported in response to extremely low pH. For example, freshwater fathead minnow (*Pimephales promelas*) exposed to pH 5.0–5.5 (manipulated using sulfuric acid) had increased ionocyte abundance on the gill filaments and lamellae (Leino et al., 1984). One potential explanation is that upregulation of ion transport by already existing ionocytes may be sufficient to deal with the stress under most environmental conditions experienced by the fish (Montgomery et al., 2022). However, intense red tides might induce an unusually larger disturbance for which fish cannot adequately compensate.

Mitigation strategies and future directions

While the effects of deteriorating red tide conditions on the local ecosystem are likely largely inevitable, early detection through community science observations and real-time monitoring can allow for potential mitigation by nearshore or onshore stakeholders utilizing local seawater (e.g., research institutions, aquaria, and aquaculture operations) that can help prevent severe negative economic consequences (Matsuyama, 1999; Hoagland and Scatasta, 2006). Early detection and real-time monitoring utilizing existing infrastructure (Bresnahan et al., 2020) likely serve as some of the most important tools to allow for preemptive or immediate adjustment to deteriorating conditions, and, in the longer term, the data generated by already-deployed instrumentation is critical for improving our understanding of these events. Imaging Flow Cytobots can detect changes in phytoplankton composition and therefore are good indicators for bloom development and decay, while oceanic sensors can help monitor hazardous oxygen and pH conditions. On larger scales, satellites can be used to detect blooms via spectral reflectance or UV reflectance ratios (Caballero et al., 2020; Kahru et al., 2021) and may prove to be a useful tool for early detection and quantification of future blooms as the technology improves, although temporal resolution is lower than in situ sensors. In addition, consistent sampling and institutional networks can greatly increase the response rate of local facilities. For instance, the California HABMAP (https://calhabmap.org/) is a statewide network in which weekly phytoplankton and water samples across multiple sites help to create an informed understanding of how the environment changes with time, and can alert users to potential developing hazardous conditions.

Due to the historic nature of this red tide and its occurrence during COVID-19 restrictions, most local stakeholder responses were reactionary and only occurred after significant biological impacts had already occurred. For example, SIO installed a new drum filter on the pier seawater intake shortly after mass mortality events that greatly reduced the amount of suspended solids that had previously made their way into aquaria tanks, clogged

other filtration systems, and exacerbated poor water conditions. Similarly, at all aquarium facilities, increased aeration within the tanks was found to help prevent more mass mortality by increasing dissolved oxygen levels, stabilizing pH, and also likely off-gassing other byproducts such as toxic nitrogenous and sulfuric compounds. Extensive aeration and supplemental oxygen were also applied to great success in the field using large, custom-built bubbling systems at aquaculture facilities offshore in Baja California Norte and in Agua Hedionda Lagoon following initial mortalities. Additionally, there was little mortality in tanks at SWFSC and the Birch Aquarium that were part of separate recirculating systems, and thus standby recirculating systems, although costly, may be an important tool for facilities to utilize during harmful algal blooms. Such recirculating systems are already used in fish and shellfish aquaculture to allow for greater water quality control, such as to shield vulnerable shellfish life stages from low pH water during seasonal upwelling.

The further development of monitoring and mitigation techniques are particularly important to the local area given the recent federal designation of the southern California region as an Aquaculture Opportunity Area for aquaculture development. Future physiological studies are thus also important to determine environmental tolerances (e.g., to hypoxia, to harmful chemical compounds, and combined stressors) to better understand the effects that red tides may have on target commercial and aquaculture species. For example, white seabass (*Atractoscion nobilis*), which are cultured in southern California as part of a stock replenishment program that was established by California State Legislature in 1983 (Ocean Resources Enhancement and Hatchery Program; FGC § 6592; FGC § 6590; California Sea Grant, 2017), experienced low mortality at Hubbs aquarium despite being a very active fish with high oxygen demands, and there was little observed mortality from this species in the wild. These findings may be explained, at least in part, by species-specific mechanisms to enhance oxygen uptake from seawater and delivery to tissues by their red blood cells (Harter et al., 2021).

Finally, while all of the sensor sites showed similar general trends in temporal red tide bloom dynamics, the intensity of adverse conditions varied greatly, resulting in wide-ranging biological impacts dependent on physical-spatial dynamics and site characteristics. For example, while the red tide encompassed coastal kelp forests, reports of mortality in these areas were limited, and the kelp and fish community assemblage appeared to be generally resilient to the surrounding harsh environmental conditions. Likewise, while certain estuaries were devastated by large-scale mortalities, others (e.g., Mission Bay, San Diego Bay) appeared to escape generally unaffected. Better understanding such spatial characteristics, hydrodynamics, and potential natural buffering and recovery capacities are particularly important for the limited and generally small estuaries found along the coast of southern California, which play an outsized role as critical nursery grounds for many fish species (Miller et al., 1985; Castro, 1993; Primo et al., 2013). While some estuarine communities have been shown to largely rebound from

mass mortality events in as short a period as one month (Reis-Filho et al., 2012), this rebound is typically dependent on seeding from other nearby estuaries. Our results from Los Peñasquitos Lagoon showed that 2.5 months post-red tide only the benthic macrofaunal sampling site closest to the ocean had recovered to pre-red tide organismal densities, and species composition continued to differ from that prior to the red tide. This recovery process is likely further complicated by heavy urbanization and frequent estuary mouth maintenance activities often required to ensure adequate ocean flushing (McLaughlin et al., 2013; Levin et al., 2022).

While southern California lagoons and embayments are known to experience hypoxic conditions naturally (Levin et al., 2022), sometimes in conjunction with red tides (Barboza and Weiss, 2011; Stauffer et al., 2012), the 2020 event described here was notable for its widespread nature and the occurrence of open coast hypoxia and associated mass mortalities, which are extremely rare for southern California coastal waters. Such widespread and protracted red tides are thus likely to have more pronounced local effects and may have disproportionate ramifications in locations such as southern California where estuaries are generally smaller and less abundant than many other coastal regions. In addition, extreme precipitation events, such as the high rainfall that occurred in March and April 2020 and helped sustain the 2020 red tide, are becoming more frequent in California (Berg and Hall, 2015; Polade et al., 2017) and, along with other factors such as ocean warming and acidification, increase the potential for future extreme red tide events (Zohdi and Abbaspour, 2019; Gobler, 2020) and compound stressors. Therefore, closer monitoring of the effect of red tides within vulnerable areas is imperative in order to further understand and potentially mitigate local community and ecosystem impacts.

Data accessibility statement
Data are available at https://figshare.com/s/7ad08e0fddd423c925d5.

Supplemental files
The supplemental files for this article can be found as follows:

Tables S1–S3. Figures S1 and S2. PDF

Competing interests
The authors have declared that no competing interests exist.

Author contributions
Contributed to conception and design: ZRS, NCW.

Contributed to acquisition of data: All authors.

Contributed to analysis and interpretation of data: ZRS, GTK, LRM, JL, SMC, JES, US, TRM, PJB, SNG, LAL, BWF, JJM, MT, NCW, CN, SJ.

Drafted and/or revised the article: All authors.

Approved the submitted version for publication: All authors.

References
Achá, D, Guédron, S, Amouroux, D, Point, D, Lazzaro, X, Fernandez, PE, Sarret, G. 2018. Algal bloom exacerbates hydrogen sulfide and methylmercury contamination in the emblematic high-altitude Lake Titicaca. *Geosciences* **8**: 438. DOI: http://dx.doi.org/10.3390/geosciences8120438.

Allen, SE, Vindeirinho, C, Thomson, RE, Foreman, MG, Mackas, DL. 2001. Physical and biological processes over a submarine canyon during an upwelling event. *Canadian Journal of Fisheries and Aquatic Sciences* **58**: 671–684. DOI: http://dx.doi.org/10.1139/f01-008.

Allen, WE. 1946. "Red water" in La Jolla Bay in 1945. *Transactions of the American Microscopical Society* **65**: 149–153. DOI: http://dx.doi.org/10.2307/3223175.

Anderson, C, Hepner-Medina, M. 2020. Red tide bulletin spring 2020. Southern California Coastal Ocean Observing System. Available at https://sccoos.org/california-hab-bulletin/red-tide/. Accessed February 26, 2023.

Anderson, DM. 1994. Red tides. *Scientific American* **271**: 62–68.

Anderson, DM, Glibert, PM, Burkholder, JM. 2002. Harmful algal blooms and eutrophication: Nutrient sources, composition, and consequences. *Estuaries* **25**: 704–726. DOI: http://dx.doi.org/10.1007/BF02804901.

Armstrong, M, Kudela, R. 2006. Evaluation of California isolates of *Lingulodinium polyedrum* for the production of yessotoxin. *African Journal of Marine Science* **28**: 399–401. DOI: http://dx.doi.org/10.2989/18142320609504186.

Bagarinao, T, Lantin-Olaguer, I. 1998. The sulfide tolerance of milkfish and tilapia in relation to fish kills in farms and natural waters in the Philippines. *Hydrobiologia* **382**: 137–150. DOI: http://dx.doi.org/10.1023/A:1003420312764.

Baohong, C, Kang, W, Xu, D, Hui, L. 2021. Long-term changes in red tide outbreaks in Xiamen Bay in China from 1986 to 2017. *Estuarine, Coastal and Shelf Science* **249**: 107095. DOI: http://dx.doi.org/10.1016/j.ecss.2020.107095.

Barboza, T, Weiss, KR. 2011 Mar 8. Redondo Beach fish die-off: Tests show oxygen levels at 'almost zero'. *Los Angeles Times*.

Becke, C, Schumann, M, Steinhagen, D, Rojas-Tirado, P, Geist, J, Brinker, A. 2019. Effects of unionized ammonia and suspended solids on rainbow trout (*Oncorhynchus mykiss*) in recirculating aquaculture systems. *Aquaculture* **499**: 348–357. DOI: http://dx.doi.org/10.1016/j.aquaculture.2018.09.048.

Berg, N, Hall, A. 2015. Increased interannual precipitation extremes over California under climate change. *Journal of Climate* **28**: 6324–6334. DOI: http://dx.doi.org/10.1175/JCLI-D-14-00624.1.

Bhatnagar, A, Devi, P. 2013. Water quality guidelines for the management of pond fish culture. *International Journal of Environmental Sciences* **3**: 1980–2009. DOI: http://dx.doi.org/10.6088/ijes.2013030600019.

Boardman, GD, Starbuck, SM, Hudgins, DB, Li, X, Kuhn, DD. 2004. Toxicity of ammonia to three marine fish and three marine invertebrates. *Environmental Toxicology: An International Journal* **19**: 134–142. DOI: http://dx.doi.org/10.1002/tox.20006.

Bresnahan, PJ, Wirth, T, Martz, T, Shipley, K, Rowley, V, Anderson, C, Grimm, T. 2020. Equipping smart coasts with marine water quality IoT sensors. *Results in Engineering* **5**: 100087. DOI: http://dx.doi.org/10.1016/j.rineng.2019.100087.

Caballero, I, Fernández, R, Escalante, OM, Mamán, L, Navarro, G. 2020. New capabilities of Sentinel-2A/B satellites combined with *in situ* data for monitoring small harmful algal blooms in complex coastal

waters. *Scientific Reports* **10**: 1–14. DOI: http://dx.doi.org/10.1038/s41598-020-65600-1.

Cai, WJ, Hu, X, Huang, WJ, Murrell, MC, Lehrter, JC, Lohrenz, SE, Chou, WC, Zhai, W, Hollibaugh, JT, Wang, Y, Zhao, P. 2011. Acidification of subsurface coastal waters enhanced by eutrophication. *Nature Geoscience* **4**: 766–770. DOI: http://dx.doi.org/10.1038/ngeo1297.

Castro, JI. 1993. The shark nursery of Bulls Bay, South Carolina, with a review of the shark nurseries of the southeastern coast of the United States. *Environmental Biology of Fishes* **38**: 37–48. DOI: http://dx.doi.org/10.1007/BF00842902.

Coutant, CC. 1987. Poor reproductive success of striped bass from a reservoir with reduced summer habitat. *Transactions of the American Fisheries Society* **116**: 154–160. DOI: http://dx.doi.org/10.1577/1548-8659(1987)116<154:PRSOSB>2.0.CO;2.

Dayton, PK, Tegner, MJ, Edwards, PB, Riser, KL. 1999. Temporal and spatial scales of kelp demography: The role of oceanographic climate. *Ecological Monographs* **69**: 219–250. DOI: http://dx.doi.org/10.1890/0012-9615(1999)069[0219:TASSOK]2.0.CO;2.

De Wit, P, Rogers-Bennett, L, Kudela, RM, Palumbi, SR. 2014. Forensic genomics as a novel tool for identifying the causes of mass mortality events. *Nature Communications* **5**: 3652. DOI: http://dx.doi.org/10.1038/ncomms4652.

Diaz, RJ, Rosenberg, R. 1995. Marine benthic hypoxia: A review of its ecological effects and the behavioural responses of benthic macrofauna. *Oceanography and Marine Biology: An Annual Review* **33**: 245–303.

Dupont, JM, Hallock, P, Jaap, WC. 2010. Ecological impacts of the 2005 red tide on artificial reef epibenthic macroinvertebrate and fish communities in the eastern Gulf of Mexico. *Marine Ecology Progress Series* **415**: 189–200. DOI: http://dx.doi.org/10.3354/meps08739.

Fennie, HW, Ben-Aderet, N, Bograd, SJ, Kwan, GT, Santora, JA, Schroeder, ID, Thompson, AR. 2023. Momma's larvae: Maternal oceanographic experience and larval size influence early survival of rockfishes. *Fisheries Oceanography.* DOI: http://dx.doi.org/10.1111/fog.12658.

Fire, SE, Van Dolah, FM. 2012. Marine biotoxins, in Aguirre, AA, Ostfield, RS, Daszak, P eds., *New directions in conservation medicine: Applied cases in ecological health.* New York, NY: Oxford University Press: 374–389.

Flaherty, KE, Landsberg, JH. 2011. Effects of a persistent red tide (*Karenia brevis*) bloom on community structure and species-specific relative abundance of nekton in a Gulf of Mexico estuary. *Estuaries and Coasts* **34**: 417–439. DOI: http://dx.doi.org/10.1007/s12237-010-9350-x.

Florida Department of Environmental Protection. 2023. Un-ionized ammonia calculator. Available at https://floridadep.gov/waste/district-business-support/documents/un-ionized-ammonia-calculator. Accessed September 06, 2023.

Franklin, DA, Edward, L. 2019. Ammonia toxicity and adaptive response in marine fishes. *Indian Journal of Geo-Marine Sciences (IJMS)* **48**: 273–279.

Frieder, CA, Nam, SH, Martz, TR, Levin, LA. 2012. High temporal and spatial variability of dissolved oxygen and pH in a nearshore California kelp forest. *Biogeosciences* **9**: 3917–3930. DOI: https://doi.org/10.5194/bg-9-3917-2012.

Froese, R, Pauly, D eds. 2023. FishBase Version (10/2023). Available at www.fishbase.org. Accessed November 19, 2023.

Frommel, AY, Kwan, GT, Prime, KJ, Tresguerres, M, Lauridsen, H, Val, AL, Gonçalves, LU, Brauner, CJ. 2021. Changes in gill and air-breathing organ characteristics during the transition from water-to air-breathing in juvenile *Arapaima gigas. Journal of Experimental Zoology Part A: Ecological and Integrative Physiology* **335**(9–10): 801–813. DOI: http://dx.doi.org/10.1002/jez.2456.

Gannon, DP, McCabe, EJB, Camilleri, SA, Gannon, JG, Brueggen, MK, Barleycorn, AA, Palubok, VI, Kirkpatrick, GJ, Wells, RS. 2009. Effects of *Karenia brevis* harmful algal blooms on nearshore fish communities in southwest Florida. *Marine Ecology Progress Series* **378**: 171–186. DOI: http://dx.doi.org/10.3354/meps07853.

Glibert, PM, Magnien, R, Lomas, MW, Alexander, J, Tan, C, Haramoto, E, Trice, M, Kana, TM. 2001. Harmful algal blooms in the Chesapeake and coastal bays of Maryland, USA: Comparison of 1997, 1998, and 1999 events. *Estuaries* **24**: 875–883. DOI: http://dx.doi.org/10.2307/1353178.

Gobler, CJ. 2020. Climate change and harmful algal blooms: Insights and perspective. *Harmful Algae* **91**: 101731. DOI: http://dx.doi.org/10.1016/j.hal.2019.101731.

Grattan, LM, Holobaugh, S, Morris, JG Jr. 2016. Harmful algal blooms and public health. *Harmful Algae* **57**: 2–8. DOI: http://dx.doi.org/10.1016/j.hal.2016.05.003.

Gravinese, PM, Munley, MK, Kahmann, G, Cole, C, Lovko, V, Blum, P, Pierce, R. 2020. The effects of prolonged exposure to hypoxia and Florida red tide (*Karenia brevis*) on the survival and activity of stone crabs. *Harmful Algae* **98**: 101897. DOI: http://dx.doi.org/10.1016/j.hal.2020.101897.

Green, BC, Smith, DJ, Grey, J, Underwood, GJ. 2012. High site fidelity and low site connectivity in temperate salt marsh fish populations: A stable isotope approach. *Oecologia* **168**: 245–255. DOI: http://dx.doi.org/10.1007/s00442-011-2077-y.

Hallegraeff, GM. 2003. Harmful algal blooms: A global overview. *Manual on Harmful Marine Microalgae* **33**: 1–22.

Hallegraeff, GM. 2010. Ocean climate change, phytoplankton community responses, and harmful algal blooms: A formidable predictive challenge. *Journal*

of Phycology **46**: 220–235. DOI: http://dx.doi.org/10.1111/j.1529-8817.2010.00815.x.

Hallett, CS, **Valesini, FJ**, **Clarke, KR**, **Hoeksema, SD.** 2016. Effects of a harmful algal bloom on the community ecology, movements and spatial distributions of fishes in a microtidal estuary. *Hydrobiologia* **763**: 267–284. DOI: http://dx.doi.org/10.1007/s10750-015-2383-1.

Hannah, RW, **Rankin, PS.** 2011. Site fidelity and movement of eight species of Pacific rockfish at a high-relief rocky reef on the Oregon coast. *North American Journal of Fisheries Management* **31**: 483–494. DOI: http://dx.doi.org/10.1080/02755947.2011.591239.

Harding, JM, **Allen, DM**, **Haffey, ER**, **Hoffman, KM.** 2020. Site fidelity of oyster reef blennies and gobies in saltmarsh tidal creeks. *Estuaries and Coasts* **43**: 409–423. DOI: http://dx.doi.org/10.1007/s12237-019-00678-z.

Harter, TS, **Brauner, CJ.** 2021. Teleost red blood cells actively enhance the passive diffusion of oxygen that was discovered by August Krogh. *Comparative Biochemistry and Physiology Part A: Molecular & Integrative Physiology* **253**: 110855. DOI: http://dx.doi.org/10.1016/j.cbpa.2020.110855.

Hickey, BM. 1995. Coastal submarine canyons, in Muller, P ed., *Topographic effects in the ocean*. Aha Hulika'a, Proceedings of the Hawaiian Winter Workshop, University of Hawaii: 95–110.

Hirsh, HK, **Nickols, KJ**, **Takeshita, Y**, **Traiger, SB**, **Mucciarone, DA**, **Monismith, S**, **Dunbar, RB.** 2020. Drivers of biogeochemical variability in a central California kelp forest: Implications for local amelioration of ocean acidification. *Journal of Geophysical Research: Oceans* **125**: e2020JC016320. DOI: http://dx.doi.org/10.1029/2020JC016320.

Hitchcock, GL, **Kirkpatrick, G**, **Lane, PV**, **Langdon, C.** 2014. Comparative diel oxygen cycles preceding and during a *Karenia* bloom in Sarasota Bay, Florida, USA. *Harmful Algae* **38**: 95–100. DOI: http://dx.doi.org/10.1016/j.hal.2014.05.010.

Hoagland, P, **Scatasta, S.** 2006. The economic effects of harmful algal blooms. *Ecology of Harmful Algae* **189**: 391–402.

Hofmann, GE, **Smith, JE**, **Johnson, KS**, **Send, U**, **Levin, LA**, **Micheli, F**, **Paytan, A**, **Price, NN**, **Peterson, B**, **Takeshita, Y**, **Matson, PG.** 2011. High-frequency dynamics of ocean pH: A multi-ecosystem comparison. *PLoS One* **6**: e28983. DOI: http://dx.doi.org/10.1371/journal.pone.0028983.

Holmes, RW, **Williams, PM**, **Eppley, RW.** 1967. Red water in La Jolla Bay, 1964–1966. *Limnology and Oceanography* **12**: 503–512. DOI: http://dx.doi.org/10.4319/lo.1967.12.3.0503.

Howard, MD, **Silver, M**, **Kudela, RM.** 2008. Yessotoxin detected in mussel (*Mytilus californicus*) and phytoplankton samples from the US west coast. *Harmful Algae* **7**: 646–652. DOI: http://dx.doi.org/10.1016/j.hal.2008.01.003.

Jin, D, **Thunberg, E**, **Hoagland, P.** 2008. Economic impact of the 2005 red tide event on commercial shellfish fisheries in New England. *Ocean & Coastal Management* **51**: 420–429. DOI: http://dx.doi.org/10.1016/j.ocecoaman.2008.01.004.

Kahle, DJ, **Wickham, H.** 2013. GGmap: Spatial visualization with ggplot2. *The R Journal* **5**: 144–161. Available at https://journal.r-project.org/archive/2013-1/kahle-wickham.pdf.

Kahru, M, **Anderson, C**, **Barton, AD**, **Carter, ML**, **Catlett, D**, **Send, U**, **Sosik, HM**, **Weiss, EL**, **Mitchell, BG**. 2021. Satellite detection of dinoflagellate blooms off California by UV reflectance ratios. *Elementa: Science of the Anthropocene* **9**: 00157. DOI: http://dx.doi.org/10.1525/elementa.2020.00157.

Kahru, M, **Mitchell, BG.** 1998. Spectral reflectance and absorption of a massive red tide off Southern California. *Journal of Geophysical Research: Oceans* **103**: 21601–21609. DOI: http://dx.doi.org/10.1029/98JC01945.

Kekuewa, SA, **Courtney, TA**, **Cyronak, T**, **Andersson, AJ.** 2022. Seasonal nearshore ocean acidification and deoxygenation in the Southern California Bight. *Scientific Reports* **12**: 17969. DOI: http://dx.doi.org/10.1038/s41598-022-21831-y.

Kreiss, CM, **Michael, K**, **Lucassen, M**, **Jutfelt, F**, **Motyka, R**, **Dupont, S**, **Pörtner, HO.** 2015. Ocean warming and acidification modulate energy budget and gill ion regulatory mechanisms in Atlantic cod (*Gadus morhua*). *Journal of Comparative Physiology B* **185**: 767–781. DOI: http://dx.doi.org/10.1007/s00360-015-0923-7.

Kwan, GT, **Finnerty, SH**, **Wegner, NC**, **Tresguerres, M.** 2019a. Quantification of cutaneous ionocytes in small aquatic organisms. *Bio-protocol* **9**: e3227. DOI: http://dx.doi.org/10.21769/BioProtoc.3227.

Kwan, GT, **Frable, BW**, **Thompson, AR**, **Tresguerres, M.** 2022. Optimizing immunostaining of archival fish samples to enhance museum collection potential. *Acta Histochemica* **124**: 151952. DOI: http://dx.doi.org/10.1016/j.acthis.2022.151952.

Kwan, GT, **Shen, SG**, **Drawbridge, M**, **Checkley, DM Jr**, **Tresguerres, M.** 2021. Ion-transporting capacity and aerobic respiration of larval white seabass (*Atractoscion nobilis*) may be resilient to ocean acidification conditions. *Science of the Total Environment* **791**: 148285. DOI: http://dx.doi.org/10.1016/j.scitotenv.2021.148285.

Kwan, GT, **Smith, TR**, **Tresguerres, M.** 2020. Immunological characterization of two types of ionocytes in the inner ear epithelium of Pacific Chub Mackerel (*Scomber japonicus*). *Journal of Comparative Physiology B* **190**: 419–431. DOI: http://dx.doi.org/10.1007/s00360-020-01276-3.

Kwan, GT, **Wexler, JB**, **Wegner, NC**, **Tresguerres, M.** 2019b. Ontogenetic changes in cutaneous and branchial ionocytes and morphology in yellowfin tuna (*Thunnus albacares*) larvae. *Journal of Comparative Physiology B* **189**: 81–95. DOI: http://dx.doi.org/10.1007/s00360-018-1187-9.

Landsberg, J, **Van Dolah, F**, **Doucette, G.** 2005. Marine and estuarine harmful algal blooms: Impacts on human and animal health, in Belkin, S, Colwell, RR eds., *Oceans and health: Pathogens in the marine environment.* New York, NY: Springer: 165–215.

Landsberg, JH. 2002. The effects of harmful algal blooms on aquatic organisms. *Reviews in Fisheries Science* **10**: 113–390. DOI: http://dx.doi.org/10.1080/20026491051695.

Lebovitz, RM, **Takeyasu, K**, **Fambrough, D.** 1989. Molecular characterization and expression of the (Na++ K+)-ATPase alpha-subunit in Drosophila melanogaster. *The EMBO Journal* **8**: 193–202. DOI: http://dx.doi.org/10.1002/j.1460-2075.1989.tb03364.x.

Leino, RL, **McCormick, JH.** 1984. Morphological and morphometrical changes in chloride cells of the gills of *Pimephales promelas* after chronic exposure to acid water. *Cell and Tissue Research* **236**: 121–128. DOI: http://dx.doi.org/10.1007/BF00216521.

Leivestad, H, **Muniz, IP.** 1976. Fish kill at low pH in a Norwegian river. *Nature* **259**: 391–392. DOI: http://dx.doi.org/10.1038/259391a0.

Lepage, D, **Vaidya, G**, **Guralnick, R.** 2014. Avibase—A database system for managing and organizing taxonomic concepts. *ZooKeys* **420**: 117–135. DOI: http://dx.doi.org/10.3897/zookeys.420.7089.

Levin, LA, **Mendoza, GF**, **Neira, C**, **Giddings, SN**, **Crooks, JA**. 2022. Consequences of mouth closure and hypoxia-induced state changes in low-inflow estuaries: Benthic community and trait-based response. *Estuaries and Coasts* **46**(8): 1–20. DOI: http://dx.doi.org/10.1007/s12237-022-01132-3.

Lewitus, AJ, **Horner, RA**, **Caron, DA**, **Garcia-Mendoza, E**, **Hickey, BM**, **Hunter, M**, **Huppert, DD**, **Kudela, RM**, **Langlois, GW**, **Largier, JL**, **Lessard, EJ.** 2012. Harmful algal blooms along the North American west coast region: History, trends, causes, and impacts. *Harmful Algae* **19**: 133–159. DOI: http://dx.doi.org/10.1016/j.hal.2012.06.009.

Low, NH, **Micheli, F**, **Aguilar, JD**, **Arce, DR**, **Boch, CA**, **Bonilla, JC**, **Bracamontes, MÁ**, **De Leo, G**, **Diaz, E**, **Enríquez, E**, **Hernandez, A.** 2021. Variable coastal hypoxia exposure and drivers across the southern California current. *Scientific Reports* **11**: 10929. DOI: http://dx.doi.org/10.1038/s41598-021-89928-4.

Magne, R, **Belibassakis, KA**, **Herbers, TH**, **Ardhuin, F**, **O'Reilly, WC**, **Rey, V.** 2007. Evolution of surface gravity waves over a submarine canyon. *Journal of Geophysical Research: Oceans* **112**: C01002. DOI: http://dx.doi.org/10.1029/2005JC003035.

Marasović, I, **Gačić, M**, **Kovačević, V**, **Krstulović, N**, **Kušpilić, G**, **Pucher-Petković, T**, **Odžak, N**, **Šolić, M.** 1991. Development of the red tide in the Kaštela Bay (Adriatic Sea). *Marine Chemistry* **32**: 375–387. DOI: http://dx.doi.org/10.1016/0304-4203(91)90050-7.

Matsuyama, Y. 1999. Harmful effect of dinoflagellate *Heterocapsa* circularisquama on shellfish aquaculture in Japan. *Japan Agricultural Research Quarterly* **33**: 283–294.

McHugh, KA, **Allen, JB**, **Barleycorn, AA**, **Wells, RS.** 2011. Severe *Karenia brevis* red tides influence juvenile bottlenose dolphin (*Tursiops truncates*) behavior in Sarasota Bay, Florida. *Marine Mammal Science* **27**: 622–643. DOI: http://dx.doi.org/10.1111/j.1748-7692.2010.00428.x.

McLaughlin, K, **Sutula, M**, **Busse, L**, **Anderson, S**, **Crooks, J**, **Dagit, R**, **Gibson, D**, **Johnston, K**, **Stratton, L.** 2013. A regional survey of the extent and magnitude of eutrophication in mediterranean estuaries of southern California, USA. *Estuaries and Coasts* **37**: 259–278. DOI: http://dx.doi.org/10.1007/s12237-013-9670-8.

Mileva, VR, **Gilmour, KM**, **Balshine, S.** 2011. Effects of maternal stress on egg characteristics in a cooperatively breeding fish. *Comparative Biochemistry and Physiology Part A: Molecular & Integrative Physiology* **158**: 22–29. DOI: https://doi.org/10.1016/j.cbpa.2010.08.017.

Miller, JM. 1985. Migration and utilization of estuarine nurseries by juvenile fishes: An evolutionary perspective. *Contributions Marine Science* **27**: 338–352.

Montgomery, DW, **Kwan, GT**, **Davison, WG**, **Finlay, J**, **Berry, A**, **Simpson, SD**, **Engelhard, GH**, **Birchenough, SN**, **Tresguerres, M**, **Wilson, RW.** 2022. Rapid blood acid–base regulation by European sea bass (*Dicentrarchus labrax*) in response to sudden exposure to high environmental CO_2. *Journal of Experimental Biology* **225**: jeb242735. DOI: http://dx.doi.org/10.1242/jeb.242735.

Munk, WH, **Traylor, MA.** 1947. Refraction of ocean waves: A process linking underwater topography to beach erosion. *The Journal of Geology* **55**: 1–26.

Neira, C, **Levin, LA**, **Wheeler, D**, **Giddings, S**, **McCullough, J**, **Gossett, R**, **Crooks, J.** 2022. Does lagoon closure alter pollutant loading with effects on faunal community structure and functional diversity? Final Report for California Department of Parks and Recreation, Natural Resources Division, March 2022.

Nezlin, NP, **Kamer, K**, **Hyde, J**, **Stein, ED.** 2009. Dissolved oxygen dynamics in a eutrophic estuary, Upper Newport Bay, California. *Estuarine, Coastal and Shelf Science* **82**: 139–151. DOI: http://dx.doi.org/10.1016/j.ecss.2009.01.004.

Nosal, AP, **Cartamil, DC**, **Long, JW**, **Lührmann, M**, **Wegner, NC**, **Graham, JB.** 2013. Demography and movement patterns of leopard sharks (*Triakis semifasciata*) aggregating near the head of a submarine canyon along the open coast of southern California, USA. *Environmental Biology of Fishes* **96**: 865–878. DOI: http://dx.doi.org/10.1007/s10641-012-0083-5.

Ochumba, PB. 1990. Massive fish kills within the Nyanza Gulf of Lake Victoria, Kenya. *Hydrobiologia* **208**: 93–99. DOI: http://dx.doi.org/10.1007/BF00008448.

Omand, MM, **Leichter, JJ**, **Franks, PJ**, **Guza, RT**, **Lucas, AJ**, **Feddersen, F.** 2011. Physical and biological processes underlying the sudden surface appearance of a red tide in the nearshore. *Limnology and*

Oceanography **56**: 787–801. DOI: http://dx.doi.org/10.4319/lo.2011.56.3.0787.

Palomares, MLD, **Pauly, D** eds. 2023. SeaLifeBase. Version (08/2023). Available at www.sealifebase.org. Accessed November 19, 2023.

Parnell, E, **Dayton, PK**, **Riser, K**, **Bulach, B.** 2020. Appendix A: Evaluation of anthropogenic impacts on the San Diego coastal kelp forest ecosystem (Biennial project report). Technical Report submitted to City of San Diego Public Utilities Department. Available at https://www.sandiego.gov/sites/default/files/kelpforestfinalreport_2018-2019.pdf. Accessed November 19, 2023.

Parnell, E, **Riser, K**, **Bulach, B**, **Dayton, PK.** 2022. Appendix A: Evaluation of anthropogenic impacts on the San Diego coastal kelp forest ecosystem (Biennial project report) 2020 to 2021. Technical Report submitted to City of San Diego Public Utilities Department. Available at https://www.sandiego.gov/sites/default/files/compressed_2020-2021_biennial_receiving_waters_monitoring_report.pdf. Accessed November 19, 2023.

Pickhardt, PC, **Folt, CL**, **Chen, CY**, **Klaue, B**, **Blum, JD.** 2002. Algal blooms reduce the uptake of toxic methylmercury in freshwater food webs. *Proceedings of the National Academy of Sciences* **99**(7): 4419–4423. DOI: http://dx.doi.org/10.1073/pnas.072531099.

Pitcher, GC, **Figueiras, FG**, **Hickey, BM**, **Moita, MT.** 2010. The physical oceanography of upwelling systems and the development of harmful algal blooms. *Progress in Oceanography* **85**(1–2): 5–32. DOI: http://dx.doi.org/10.1016/j.pocean.2010.02.002.

Pitcher, GC, **Foord, CJ**, **Macey, BM**, **Mansfield, L**, **Mouton, A**, **Smith, ME**, **Osmond, SJ**, **van der Molen, L.** 2019. Devastating farmed abalone mortalities attributed to yessotoxin-producing dinoflagellates. *Harmful Algae* **81**: 30–41. DOI: http://dx.doi.org/10.1016/j.hal.2018.11.006.

Polade, SD, **Gershunov, A**, **Cayan, DR**, **Dettinger, MD**, **Pierce, DW.** 2017. Precipitation in a warming world: Assessing projected hydro-climate changes in California and other Mediterranean climate regions. *Scientific Reports* **7**: 10783. DOI: http://dx.doi.org/10.1038/s41598-017-11285-y.

Primo, AL, **Azeiteiro, UM**, **Marques, SC**, **Martinho, F**, **Baptista, J**, **Pardal, MA.** 2013. Colonization and nursery habitat use patterns of larval and juvenile flatfish species in a small temperate estuary. *Journal of Sea Research* **76**: 126–134. DOI: http://dx.doi.org/10.1016/j.seares.2012.08.002.

Rankin, PS, **Hannah, RW**, **Blume, MT.** 2013. Effect of hypoxia on rockfish movements: Implications for understanding the roles of temperature, toxins and site fidelity. *Marine Ecology Progress Series* **492**: 223–234. DOI: http://dx.doi.org/10.3354/meps10479.

Reis-Filho, JA, **da Silva, EM**, **de Anchieta, C**, **da Costa Nunes, J**, **Barros, F.** 2012. Effects of a red tide on the structure of estuarine fish assemblages in northeastern Brazil. *International Review of Hydrobiology* **97**: 389–404. DOI: http://dx.doi.org/10.1002/iroh.201101457.

Richards, JG. 2011. Physiological, behavioral and biochemical adaptations of intertidal fishes to hypoxia. *Journal of Experimental Biology* **214**(2): 191–199. DOI: http://dx.doi.org/10.1242/jeb.047951.

Roberts, H, **Palmeiro, BS.** 2008. Toxicology of aquarium fish. *Veterinary Clinics of North America: Exotic Animal Practice* **11**: 359–374. DOI: http://dx.doi.org/10.1016/j.cvex.2007.12.005.

Santhosh, B, **Singh, NP.** 2007. Guidelines for water quality management for fish culture in Tripura. ICAR Research Complex for NEH Region, Tripura Center, Publication no. 29.

Schindelin, J, **Arganda-Carreras, I**, **Frise, E**, **Kaynig, V**, **Longair, M**, **Pietzsch, T**, **Preibisch, S**, **Rueden, C**, **Saalfeld, S**, **Schmid, B**, **Tinevez, JY.** 2012. Fiji: An open-source platform for biological-image analysis. *Nature Methods* **9**: 676–682. DOI: http://dx.doi.org/10.1038/nmeth.2019.

Scholin, CA, **Gulland, F**, **Doucette, GJ**, **Benson, S**, **Busman, M**, **Chavez, FP**, **Cordaro, J**, **DeLong, R**, **De Vogelaere, A**, **Harvey, J**, **Haulena, M.** 2000. Mortality of sea lions along the central California coast linked to a toxic diatom bloom. *Nature* **403**: 80–84. DOI: http://dx.doi.org/10.1038/47481.

Schreck, CB. 2010. Stress and fish reproduction: The roles of allostasis and hormesis. *General and Comparative Endocrinology* **165**: 549–556. DOI: https://doi.org/10.1016/j.ygcen.2009.07.004.

Schreck, CB, **Contreras-Sanchez, W**, **Fitzpatrick, MS.** 2001. Effects of stress on fish reproduction, gamete quality, and progeny, in Lee, C-S, Donaldson, EM eds., *Reproductive biotechnology in finfish aquaculture*: 3–24. DOI: https://doi.org/10.1016/B978-0-444-50913-0.50005-9.

Scripps Ocean Acidification Real-Time (SOAR) Monitoring Program. 2023. Available at https://coralreefecology.ucsd.edu/research/scrippsoceanacidificationreal-timesoarmonitoringprogram/. Accessed September 15, 2023.

Shipley, K, **Martz, T**, **Bresnahan, P**, **Wirth, T.** 2022. Metabolic rates in the Agua Hedionda Lagoon during the 2020 Southern California red tide event. *Elementa: Science of the Anthropocene* **10**: 00018. DOI: http://dx.doi.org/10.1525/elementa.2022.00018.

Southwest Fisheries Science Center. 2020. Animal Care and Use Committee Fish and Invertebrate Protocol #SW2001: Temperature effects on sardine metabolism and growth. Available at https://figshare.com/s/7ad08e0fddd423c925d5. Accessed January 08, 2024.

Starr, RM, **Wendt, DE**, **Barnes, CL**, **Marks, CI**, **Malone, D**, **Waltz, G**, **Schmidt, KT**, **Chiu, J**, **Launer, AL**, **Hall, NC**, **Yochum, N.** 2015. Variation in responses of fishes across multiple reserves within a network of marine protected areas in temperate waters. *PLoS One* **10**: e0118502. DOI: http://dx.doi.org/10.1371/journal.pone.0118502.

Stauffer, BA, **Gellene, AG**, **Schnetzer, A**, **Seubert, EL**, **Oberg, C**, **Sukhatme, GS**, **Caron, DA.** 2012. An oceanographic, meteorological, and biological 'perfect storm' yields a massive fish kill. *Marine Ecology Progress Series* **468**: 231–243. DOI: http://dx.doi.org/10.3354/meps09927.

Ternon, E, **Carter, ML**, **Cancelada, L**, **Lampe, RH**, **Allen, AE**, **Anderson, CR**, **Prather, KA**, **Gerwick, WH**. 2023. Yessotoxin production and aerosolization during the unprecedented red tide of 2020 in southern California. *Elementa: Science of the Anthropocene* **11**(1): 00021.

Timmons, MB, **Ebeling, JM**. 2013. *Recirculating aquaculture*. 3rd ed. Ithaca, NY: Ithaca Publishing Company LLC.

Torrey, HB. 1902. An unusual occurrence of dinoflagellate on the California coast. *The American Naturalist* **36**(423): 187–192.

Vaquer-Sunyer, R, **Duarte, CM.** 2008. Thresholds of hypoxia for marine biodiversity. *Proceedings of the National Academy of Sciences* **105**(40): 15452–15457. DOI: http://dx.doi.org/10.1073/pnas.0803833105.

Wegner, NC, **Sepulveda, CA**, **Aalbers, SA**, **Graham, JB.** 2013. Structural adaptations for ram ventilation: Gill fusions in scombrids and billfishes. *Journal of Morphology* **274**(1): 108–120. DOI: http://dx.doi.org/10.1002/jmor.20082.

Wells, ML, **Trainer, VL**, **Smayda, TJ**, **Karlson, BS**, **Trick, CG**, **Kudela, RM**, **Ishikawa, A**, **Bernard, S**, **Wulff, A**, **Anderson, DM**, **Cochlan, WP.** 2015. Harmful algal blooms and climate change: Learning from the past and present to forecast the future. *Harmful Algae* **49**: 68–93. DOI: http://dx.doi.org/10.1016/j.hal.2015.07.009.

Wickham, H, **Chang, W**, **Wickham, MH.** 2016. Package 'ggplot2'. Create elegant data visualisations using the grammar of graphics. Version 2: 1–189. Available at https://github.com/tidyverse/ggplot2. Accessed November 19, 2023.

Wilson, JM, **Erazo, N**, **Connors, E**, **Chamberlain, EJ**, **Clements, SM**, **Carter, ML**, **Smith, JE**, **Bowman, JS.** 2022. Substantial microbial community shifts in response to an exceptional harmful algal bloom in coastal Southern California. *Elementa: Science of the Anthropocene* **10**(1): 00088. DOI: http://dx.doi.org/10.1525/elementa.2021.00088.

Zheng, B, **Lucas, AJ**, **Franks, PJ**, **Schlosser, TL**, **Anderson, CR**, **Send, U**, **Davis, K**, **Barton, AD**, **Sosik, HM.** 2023. Dinoflagellate vertical migration fuels an intense red tide. *Proceedings of the National Academy of Sciences* **120**(36): e2304590120. DOI: http://dx.doi.org/10.1073/pnas.2304590120.

Zohdi, E, **Abbaspour, M.** 2019. Harmful algal blooms (red tide): A review of causes, impacts and approaches to monitoring and prediction. *International Journal of Environmental Science and Technology* **16**: 1789–1806. DOI: http://dx.doi.org/10.1007/s13762-018-2108-x.